Article

Immunity

LAG-3 Inhibitory Receptor Expression Identifies Immunosuppressive Natural Regulatory Plasma Cells

Graphical Abstract

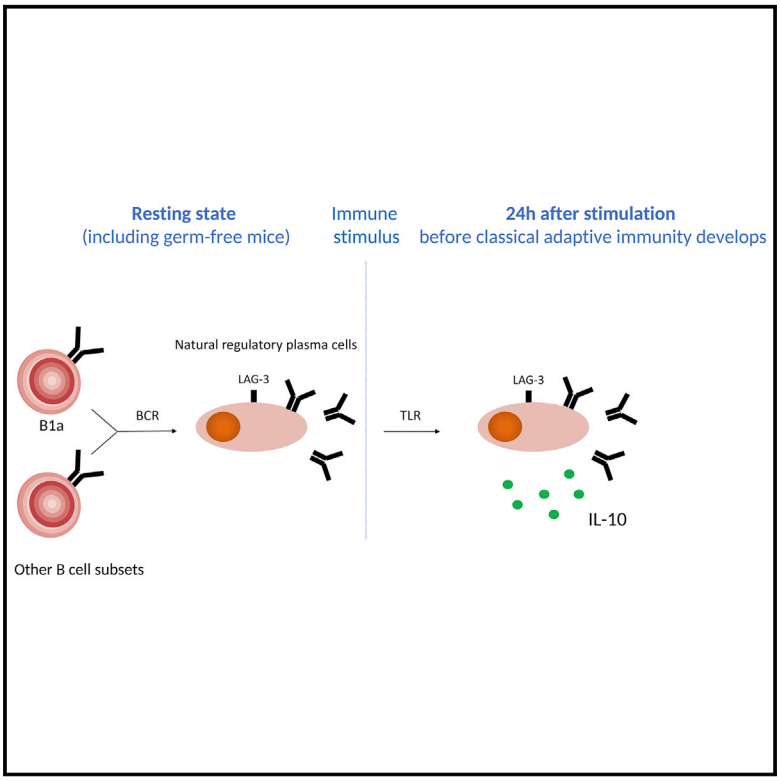

Authors

Andreia C. Lino, Van Duc Dang, Vicky Lampropoulou, ..., Stefan H.E. Kaufmann, Jörn Walter, Simon Fillatreau

Correspondence

simonfillatreau@googlemail.com

In Brief

Plasma cells secrete antibodies and play a key role in host defense against infection. Lino et al. identify a novel subset of natural regulatory plasma cells characterized by the expression of LAG-3 that develops at steady state independently of microbiota, and respond to innate stimulation by producing immunosuppressive IL-10.

Highlights

- LAG-3 expression identifies natural regulatory plasma cells
- LAG-3^{+}CD138^{hi} plasma cells express IL-10 within hours of stimulation
- LAG-3^{+}CD138^{hi} plasma cells have a unique epigenome poised to express IL-10
- LAG-3^{+}CD138^{hi} plasma cells develop via an antigen-specific mechanism

Lino et al., 2018, Immunity *49*, 120–133
July 17, 2018
https://doi.org/10.1016/j.immuni.2018.06.007

CellPress

CellPress

Immunity
Article

LAG-3 Inhibitory Receptor Expression Identifies Immunosuppressive Natural Regulatory Plasma Cells

Andreia C. Lino,[1,13] Van Duc Dang,[1,13] Vicky Lampropoulou,[1,14] Anna Welle,[2,14] Jara Joedicke,[1] Jelka Pohar,[3] Quentin Simon,[3] Jessie Thalmensi,[3] Aurelia Baures,[3] Vinciane Flühler,[3] Imme Sakwa,[1] Ulrik Stervbo,[1] Stefanie Ries,[1] Luc Jouneau,[4] Pierre Boudinot,[4] Takeshi Tsubata,[5] Takahiro Adachi,[5] Andreas Hutloff,[1] Thomas Dörner,[1,6] Ursula Zimber-Strobl,[7] Alex F. de Vos,[8] Katja Dahlke,[9] Gunnar Loh,[9] Sarantis Korniotis,[3] Christian Goosmann,[10] Jean-Claude Weill,[3] Claude-Agnès Reynaud,[3] Stefan H.E. Kaufmann,[10] Jörn Walter,[2] and Simon Fillatreau[1,3,11,12,15,*]

[1]Deutsches Rheuma-Forschungszentrum, a Leibniz Institute, Charitéplatz 1, 10117 Berlin, Germany
[2]Department of EpiGenetics, Saarland University, Campus A2.4, Saarbrücken 66123, Germany
[3]Institut Necker-Enfants Malades, INSERM U1151-CNRS UMR 8253, Paris, France
[4]Virologie et Immunologie Moléculaires, INRA, Université Paris-Saclay, 78352 Jouy-en-Josas, France
[5]Department of Immunology, Medical Research Institute, Tokyo Medical and Dental University, Tokyo 113-8510, Japan
[6]Department Medicine/Rheumatology and Clinical Immunology, Charite Universitätsmedizin Berlin, Germany
[7]Department of Gene Vectors, Helmholtz Center Munich, Marchioninistrasse 25, 81377 Munich, Germany
[8]Center for Experimental and Molecular Medicine, Academic Medical Center, University of Amsterdam, Amsterdam, the Netherlands
[9]German Institute of Human Nutrition Potsdam-Rehbruecke, Department of Gastrointestinal Microbiology, 14558 Nuthetal, Germany
[10]Max Planck Institute of Infection Biology, Charitéplatz 1, 10117 Berlin, Germany
[11]Université Paris Descartes, Sorbonne Paris Cité, Faculté de Médecine, Paris, France
[12]AP-HP, Hôpital Necker Enfants Malades, Paris, France
[13]These authors contributed equally
[14]These authors contributed equally
[15]Lead Author
*Correspondence: simonfillatreau@googlemail.com
https://doi.org/10.1016/j.immuni.2018.06.007

SUMMARY

B lymphocytes can suppress immunity through interleukin (IL)-10 production in infectious, autoimmune, and malignant diseases. Here, we have identified a natural plasma cell subset that distinctively expresses the inhibitory receptor LAG-3 and mediates this function *in vivo*. These plasma cells also express the inhibitory receptors CD200, PD-L1, and PD-L2. They develop from various B cell subsets in a B cell receptor (BCR)-dependent manner independently of microbiota in naive mice. After challenge they upregulate IL-10 expression via a Toll-like receptor-driven mechanism within hours and without proliferating. This function is associated with a unique transcriptome and epigenome, including the lowest amount of DNA methylation at the *Il10* locus compared to other B cell subsets. Their augmented accumulation in naive mutant mice with increased BCR signaling correlates with the inhibition of memory T cell formation and vaccine efficacy after challenge. These natural regulatory plasma cells may be of broad relevance for disease intervention.

INTRODUCTION

The immune system protects the host from infectious diseases and helps to remove its damaged components. Its activity is controlled by stimulatory and inhibitory forces. Inhibitory pathways are important to prevent its spontaneous hyperactivation and to regulate established immune reactions.

B lymphocytes have emerged as important players in the negative regulation of immunity via the production of interleukin-10 (IL-10) and IL-35 (Fillatreau et al., 2002; Shen and Fillatreau, 2015). This B cell function has noticeable effects in autoimmune, allergic, infectious, and malignant diseases (Shen and Fillatreau, 2015). The phenomenology of B cell-mediated suppression is well established, yet the B cells mediating these activities *in vivo* remain incompletely defined. Their identification has been approached by isolating known B cell subsets and assessing their capacity to produce IL-10 *in vitro* and to suppress immunity in recipient mice upon adoptive transfer. B cells expressing high amounts of CD1d, including marginal zone B cells and transitional T2-like B cells, as well as B1a cells and Tim-1^{hi} B cells, have the capacity to suppress immunity in an IL-10-dependent manner in such assays (Blair et al., 2009; Yanaba et al., 2008; Yang et al., 2012). However, only a fraction of the cells within these subsets express IL-10 after activation *in vitro*, even when strong pharmacological agents such as ionomycin and phorbol myristate acetate (PMA) are used, and the phenotype of the B cells actually producing IL-10 *in vivo* in the recipient is not defined after transfer. Other studies have used IL-10 reporter mice to identify IL-10-producing cells *ex vivo* without re-stimulation. These have revealed CD138^{hi} plasmocytes (plasmablasts and plasma cells) as the major source of B cell-derived IL-10 *in vivo* in autoimmune, infectious, and malignant diseases (Matsumoto et al., 2014; Neves et al., 2010; Shalapour et al., 2015; Shen et al., 2014; Teichmann et al., 2012). A hypothesis reconciling these findings could be

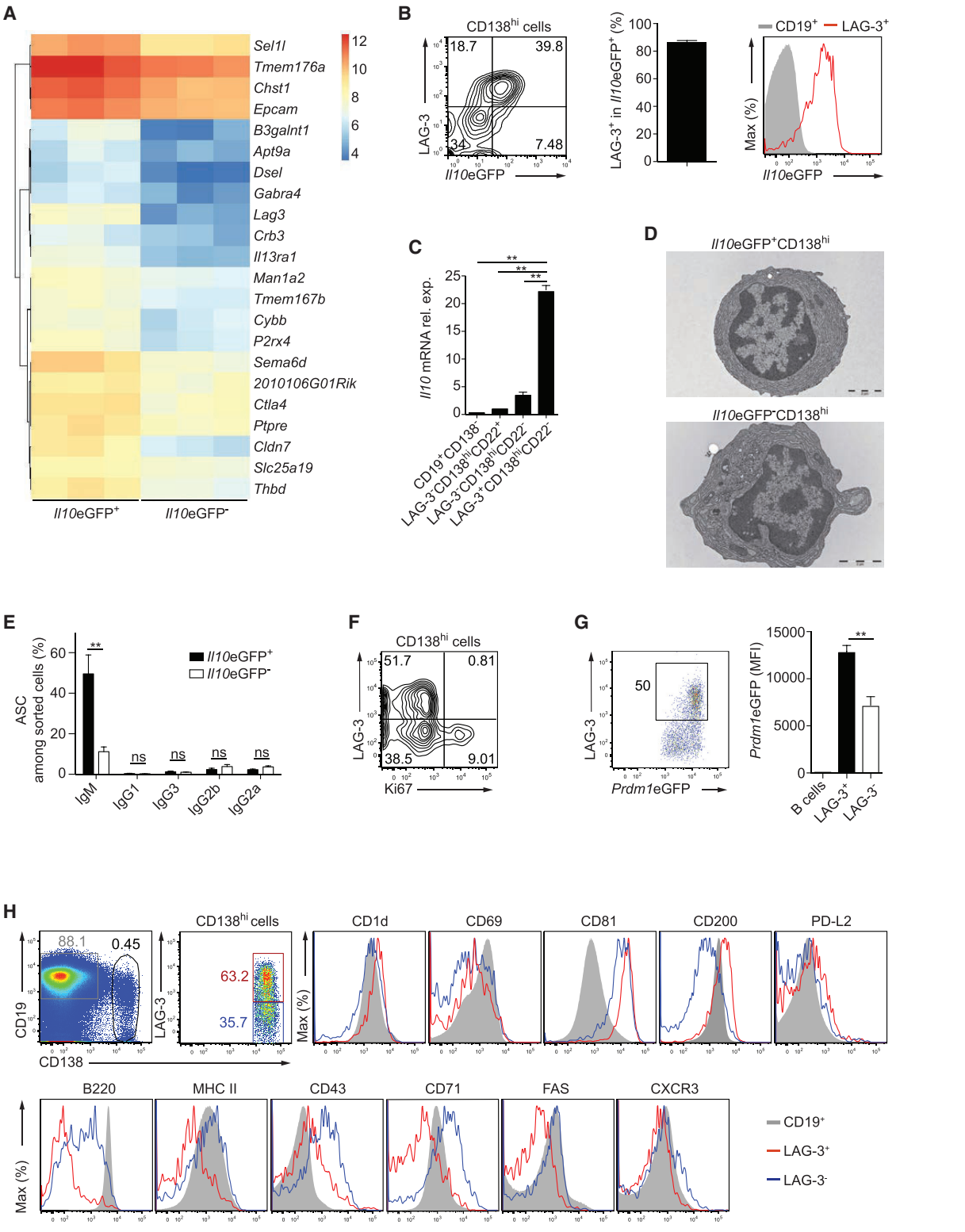

Figure 1. LAG-3 Identifies IL-10-Producing Plasma Cells in Infected Mice

Mice were infected i.v. with *Salmonella* (SL7207, 10^7 CFU), and plasmocytes characterized in spleen on day 1 p.i.

(A) mRNA amounts for receptors overexpressed in IL-10^+ compared with IL-10^- plasmocytes from *Il10*eGFP mice. Microarrays in triplicate. Expression amounts normalized using GCRMA are shown (Log2 transformed). *Lag3* is expressed 9.4-fold higher in *Il10*eGFP$^+$CD138^{hi} than *Il10*eGFP$^-$CD138^{hi} cells.

(legend continued on next page)

that B cell-mediated regulation is an inducible function acquired by B cells such as CD1d^{hi} B cells upon activation and differentiation into IL-10- or IL-35-producing plasmocytes.

Here, we addressed whether IL-10-producing plasmocytes defined a separate subset using a model of infection by the bacterium *Salmonella* Typhimurium. In this model, B cell-derived IL-10 is produced exclusively by plasmocytes that emerge before day 1 post-infection (p.i.) and leads to a rapid modulation of immunity to *Salmonella* (Neves et al., 2010). We reasoned that the rapidity of this response would facilitate the identification of the precursors of immunosuppressive IL-10-producing plasmocytes without having to recourse to adoptive transfer protocols susceptible to creating non-physiological cellular responses.

RESULTS

LAG-3 Identifies IL-10-Expressing Plasma Cells in Infected Mice

Salmonella infection results in the rapid appearance of IL-10^{+}CD138^{hi} cells. To assess whether these cells defined a particular subset, we compared their transcriptome to the one of IL-10^{-}CD138^{hi} cells from *Il10*eGFP mice on day 1 p.i. This yielded 22 genes coding for transmembrane receptors overexpressed in IL-10^{+} cells (Figure 1A), including lymphocyte-activation gene 3 (*Lag3*; CD223) that was previously identified as a marker for IL-10-producing T regulatory type (Tr1) cells (Gagliani et al., 2013).

LAG-3 protein was found on most IL-10^{+}CD138^{hi} cells on day 1 p.i., and IL-10 was expressed uniformly in LAG-3^{+}CD138^{hi} cells (Figure 1B). LAG-3 was not detected on CD19^{+}CD138^{-} cells (Figure S1A). This staining was specific because it was not observed on *Lag3*$^{-/-}$ plasma cells (Figure S1B). Consistently, *Il10* mRNA was predominantly expressed in LAG-3^{+}CD138^{hi} cells compared to other B cell subsets in infected C57BL/6 mice (Figure 1C).

IL-10^{+}LAG-3^{+}CD138^{hi} cells displayed typical plasma cell features including a plasmacytoid morphology (Figure 1D), the spontaneous secretion of antibodies (Figure 1E), a non-proliferative state (Figure 1F), and an elevated expression of BLIMP-1 (Figure 1G). LAG-3^{+}CD138^{hi} cells also differed from LAG-3^{-}CD138^{hi} cells in their higher expression of CD1d and CD200, as well as their lower expression of B220, MHC-II, CD43, CD71, and Fas (Figure 1H).

We conclude that LAG-3^{+}CD138^{hi} plasma cells define the main population of IL-10-expressing B cells in infected mice.

LAG-3^{+}CD138^{hi} Plasma Cells Develop Independently of Microbe-Derived Signals in Naive Mice

The non-proliferating status of IL-10^{+}LAG-3^{+}CD138^{hi} cells was unexpected because B cell differentiation into plasma cell normally requires cell proliferation over several days. This led us to hypothesize that LAG-3^{+}CD138^{hi} cells were already present in naive mice. Indeed, LAG-3^{+}CD138^{hi} cells were detected in the spleen, bone marrow (BM), and mesenteric lymph nodes (mLN) of naive mice (Figures 2A and S2A). They had the key attributes of plasma cells such as high BLIMP-1 expression (Figures 2B and S2B), a plasmacytoïd morphology (Figure 2C), and the spontaneous secretion of antibodies (Figure 2D). In contrast to proliferating LAG-3^{-}CD138^{hi} plasmablasts, LAG-3^{+}CD138^{hi} cells were non-proliferative and produced mostly IgM (Figures 2D and 2E). These features of LAG-3^{+}CD138^{hi} cells therefore did not change between day 0 and day 1 p.i., except for the induction of IL-10 expression after challenge (Figure 2F). LAG-3^{+}CD138^{hi} cells also differed from LAG-3^{-}CD138^{hi} cells in their higher expression of CD1d, CD69, CD81, CD200, and CD273 (PD-L2), as well as their lower expression of B220, MHC-II, CD43, CD71, FAS, and CXCR3 in naive mice (Figure 2G). PD-L1 was highly expressed by both plasmocyte subsets. LAG-3^{+}CD138^{hi} cells expressed surface IgM, CD79α, and CD79β (Figure 2G). LAG-3 expression was not observed on B cells (Figure S2C).

Plasma cells are normally induced upon foreign antigen stimulation. LAG-3^{+}CD138^{hi} cells, however, were present in similar numbers in germ-free and specific-pathogen-free mice (Figure 2H). These cells are therefore generated via an endogenous response. Their number increased markedly in aging mice (Figures 2I and S2D).

We conclude that, in naive mice, LAG-3^{+}CD138^{hi} cells are a subset of natural plasma cells mainly producing IgM.

LAG-3^{+}CD138^{hi} Cells Rapidly Upregulate IL-10 after Infection

IL-10 expression in CD138^{hi} cells increased already at 3 hr p.i. compared to naive mice ($p = 0.0009$; unpaired t test) (Figure 3A). IL-10 was expressed predominantly in LAG-3^{+}CD138^{hi} cells during the first 24 hr p.i. (Figure 3A). IL-10 is thus programmed for a rapid expression in LAG-3^{+}CD138^{hi} cells, whose numbers were similar at day 0 and day 1 p.i. (Figure 3B). As expected, IL-10 and LAG-3 were not detected in CD19^{+}CD138^{-} B cells (Figure S3A).

The immediate upregulation of IL-10 in LAG-3^{+}CD138^{hi} cells led us to compare the capacity of CD138^{hi} cells and other B cell subsets to produce IL-10 *in vitro*. CD138^{hi} plasmocytes secreted markedly more IL-10 than CD1d^{hi}CD19^{+} B cells (Figure 3C), and their IL-10 production derived mostly from LAG-3^{+}CD138^{hi} cells (Figure 3C).

We then examined IL-10 expression at later time points p.i. during the extra-follicular response. The number of CD138^{hi} cells increased progressively p.i., and they represented 10% of all

(B) Flow cytometry plots showing IL-10 and LAG-3 expression in CD138^{hi} cells (left); frequency of LAG-3^{+} in IL-10^{+}CD138^{hi} cells (middle); expression of IL-10 in B cells (CD19^{+}CD138^{-}) and LAG-3^{+}CD138^{hi} cells (right). Representative of six experiments.
(C) *Il10* mRNA expression in isolated subsets from C57BL/6 mice. Pool of two experiments.
(D) Transmission electron microscopy images of plasmocytes from *Il10*eGFP mice. Scale bar is 2 μM.
(E) Frequencies of antibody-secreting cells (ASCs) in IL-10^{+}CD138^{hi} and IL-10^{-}CD138^{hi} cells from *Il10*eGFP mice by ELISPOT. Pool of three experiments.
(F) Flow cytometry plots of LAG-3 and Ki67 expression in CD138^{hi} cells from C57BL/6 mice. Representative of four experiments.
(G) Flow cytometry plot of LAG-3 and BLIMP-1 in BLIMP-1^{+}CD138^{hi} cells (left), and amounts of BLIMP-1 (MFI) in B cells and plasmocytes in *Prdm1*eGFP mice ($n = 4$) (right). Representative of two experiments.
(H) Surface molecules expression on LAG-3^{+}CD138^{hi} (red), LAG-3^{-}CD138^{hi} (blue), and CD19^{+}CD138^{-} B cells (gray) from C57BL/6 mice. Representative of two experiments.
Data show mean ± SEM ($^{ns}p > 0.05$, $^{**}p < 0.01$). See also Figure S1.

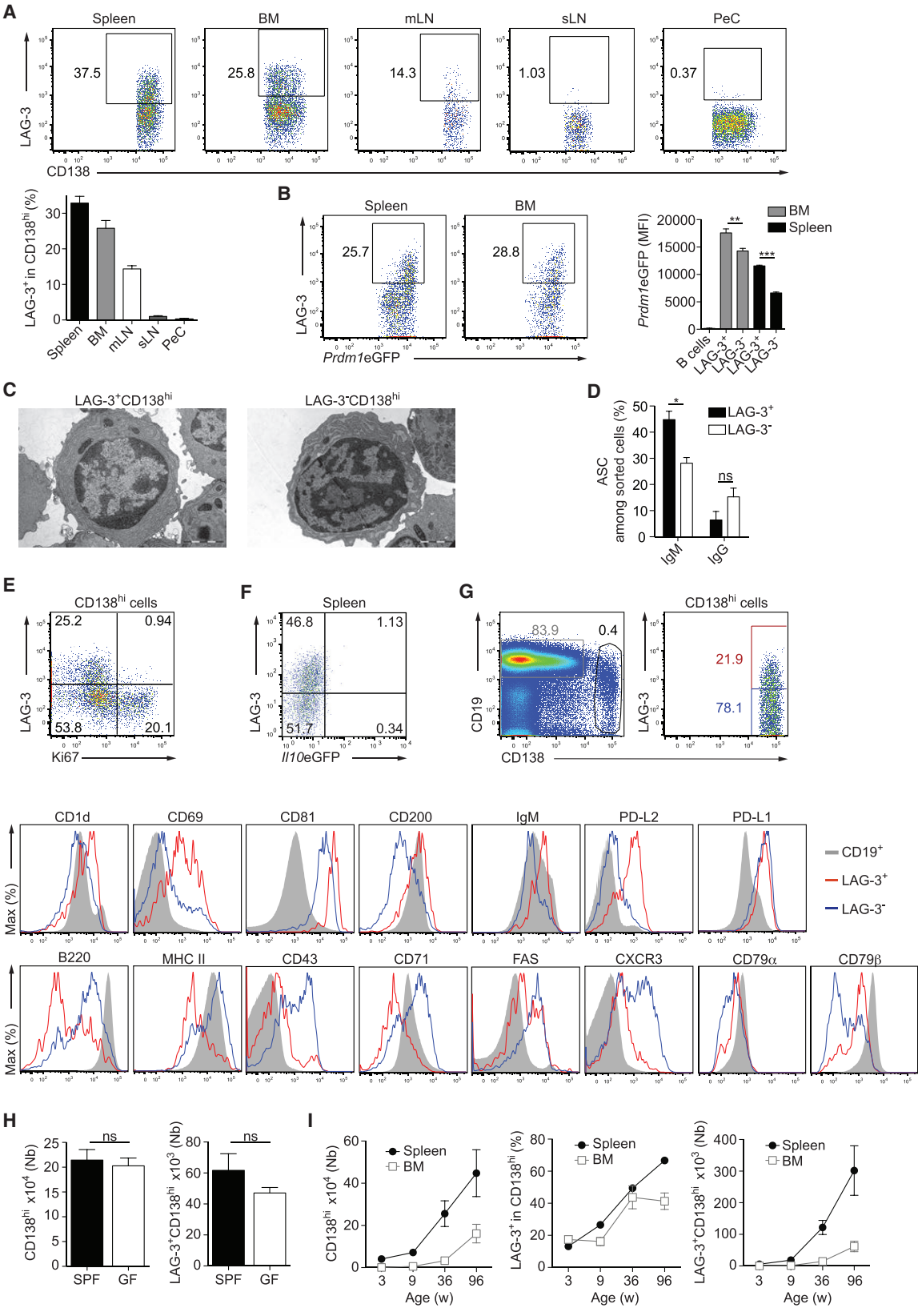

(legend on next page)

splenocytes on day 8 p.i. (Figures 3D and S3B). This increase reflected the accumulation of LAG-3^{-}CD138^{hi} cells, while IL-10^{+}LAG-3^{+}CD138^{hi} cells did not expand greatly after day 1 p.i. (Figure 3D). IL-10 expression was associated with LAG-3^{+}CD138^{hi} cells at all time points (Figure S3C). The frequencies of LAG-3^{+} and IL-10^{+} cells within CD138^{hi} cells sharply decreased from day 1 p.i. onward (Figure 3D). These results emphasize the unique response dynamics of IL-10^{+}LAG-3^{+}CD138^{hi} cells. Because LAG-3 has been implicated in the regulation of humoral immunity (Butler et al., 2011), we asked whether LAG-3 expressed on CD138^{hi} cells modulated the plasmocyte response p.i. To this end, we crossed *Lag3*$^{-/-}$ mice on an *Il10*eGFP background and generated mixed bone marrow chimera in which only B cells lacked *Lag3* but could express *Il10*eGFP. A LAG-3 deficiency in plasma cells did not alter the number of IL-10^{+}CD138^{hi} cells p.i., yet led to an increased accumulation of IL-10^{-}CD138^{hi} cells (Figure 3E). Thus, LAG-3^{+}CD138^{hi} cells control the expansion of LAG-3^{-}CD138^{hi} cells in a LAG-3-dependent manner.

An important property of the adaptive immune system is immunological memory. To assess whether LAG-3^{+}CD138^{hi} cells acquire features of memory B cells, we compared their response in vaccinated and naive mice p.i. As expected, vaccinated mice better controlled *Salmonella* than naive mice (Figure S3D). IL-10 and LAG-3 expression in CD138^{hi} cells were comparable in the two groups p.i. (Figures 3F and 3G). Thus, LAG-3^{+}CD138^{hi} cells did not display the typical sign of an amplified response upon rechallenge. IL-10^{+}CD138^{hi} cells isolated from vaccinated mice on day 1 p.i. produced mostly IgM (Figure 3H), indicating that they had not undergone isotype switching away from IgM, unlike what is observed in classical memory B cell responses.

These data show that LAG-3^{+}CD138^{hi} cells can rapidly upregulate IL-10 expression without dividing, and inhibit the expansion of LAG-3^{-}CD138^{hi} cells p.i.

LAG-3^{+}CD138^{hi} Cells Have a Unique Plasma Cell Epigenome

We next examined the hypothesis that LAG-3^{+}CD138^{hi} cells were a distinct subset of plasma cells epigenetically poised to rapidly produce IL-10. To this end, we compared the genome-wide DNA-methylomes of LAG-3^{+}CD138^{hi} cells, LAG-3^{-}CD138^{hi} cells, and peripheral B cell subsets from naive mice. In addition, we included LAG-3^{+}CD138^{hi}, LAG-3^{-}CD138^{hi}, IL-10^{+}CD138^{hi}, and IL-10^{-}CD138^{hi} cells isolated at day 1 p.i.

Genome-wide DNA-methylation profiling was performed by reduced representation bisulfite sequencing (RRBS) covering on average 3–4 million CpG sites per sample. An unsupervised principal component analysis (PCA) placed LAG-3^{+}CD138^{hi} and IL-10^{+}CD138^{hi} cells at a distinctive position relative to LAG-3^{-}CD138^{hi} and IL-10^{-}CD138^{hi} cells, as well as to other B cell subsets, underlying their unique methylome profile. The position of LAG3^{+}CD138^{hi} cells taken at day 0 and day 1 p.i. was similar and showed a striking co-localization with IL-10^{+}CD138^{hi} cells (Figure 4A), underlining the intimate relationship between these subsets. The various groups of CD138^{hi} cells localized at the same position on PC1, which separated B cells from plasma cells. In keeping with the described hypomethylation of plasma cells' genome (Kulis et al., 2015), the various CD138^{hi} subsets analyzed here displayed the lowest degree of genome-wide methylation (Figure S4A). Thus, LAG-3^{+}CD138^{hi} and IL-10^{+}CD138^{hi} cells have a plasma cell epigenetic profile but with unique features. A pairwise comparison of LAG-3^{+}CD138^{hi} and LAG-3^{-}CD138^{hi} cells from naive mice identified 469 differentially methylated regions (DMRs) showing a genome-wide distribution (Figure S4B). In a hierarchical analysis, these DMRs separated CD138^{hi} cells and B1 cells away from the other B cell subsets (Figure 4B), with LAG-3^{+}CD138^{hi} cells showing the highest similarity to B1a cells (Figures 4B and S4C). A particular cluster of DMRs was found at the *Il10* locus. IL-10^{+}CD138^{hi} cells, LAG-3^{+}CD138^{hi} cells, and B1a cells not only exhibited the lowest overall degree of DNA methylation at the *Il10* locus (Figure 4C) but also shared distinct patterns of hypomethylated regions around the *Il10* gene. Many of these hypomethylated sites overlapped with B cell-specific DNase hypersensitive sites, indicating an epigenetic "preprogrammed" open chromatin state of *Il10* in IL-10^{+}CD138^{hi}, LAG-3^{+}CD138^{hi}, and B1a cells (Figures 4D and S4D). Of note, IL-10^{+}CD138^{hi} cells, LAG-3^{+}CD138^{hi} cells, and B1a cells also showed a preferential epigenetic relationship at the 469 DMR (Figure S4E).

In summary, LAG-3^{+}CD138^{hi} cells are the epigenetically primed precursors of IL-10^{+}LAG-3^{+}CD138^{hi} cells and show a distinct plasma cell-specific epigenome with the *Il10* locus primed for expression and features reminiscent of B1a cells.

Transcriptional Properties of LAG-3^{+}CD138^{hi} Cells

We next determined the transcriptomes of LAG-3^{+}CD138^{hi} and LAG-3^{-}CD138^{hi} cells on day 0 and day 1 p.i by mRNaseq. These analyses identified 648 differentially expressed genes (DEGs) (pval $\leq$ 0.01; FDR $\leq$ 0.05) on day 0 and 2,280 on day 1 p.i.

Figure 2. LAG-3^{+}CD138^{hi} Plasma Cells Are Present in Naive Mice

Analyses performed in spleen (except when indicated) of naive mice.

(A) Flow cytometry plots of LAG-3 on CD138$^{+/hi}$ cells (top) and frequencies in spleen (n = 23), BM (n = 19), mLN (n = 10), subcutaneous LN (sLN) (n = 10), and PeC (n = 10) (bottom) of C57BL/6 mice.

(B) Flow cytometry plots of LAG-3 and BLIMP-1 in BLIMP-1^{+}CD138^{hi} cells (left), and amounts of BLIMP-1 (MFI) in B cells and plasmocytes in *Prdm1*eGFP mice (n = 4) (right). Representative of three experiments.

(C) Electron microscopy images of plasmocytes from C57BL/6 mice. Scale bar is 2 μM.

(D) ASCs in plasmocytes from C57BL/6 mice by ELISPOT. Pool of two experiments.

(E) Flow cytometry plot of LAG-3 and Ki67 in CD138^{hi} cells from C57BL/6 mice. Representative of four experiments.

(F) Flow cytometry plot of LAG-3 and IL-10 in CD138^{hi} cells. Representative of six experiments.

(G) Expression of indicated molecules on cells from C57BL/6 mice. Representative of 3–4 experiments.

(H) Numbers of plasmocytes in SPF (n = 8) and GF (n = 8) C3H/HeOuJ mice.

(I) Numbers and frequencies of plasmocytes in C57BL/6 mice of indicated ages (n = 6/age, pool of 2 experiments).

Data show mean ± SEM ($^{ns}p > 0.05$, $^{*}p < 0.05$, $^{**}p < 0.01$; $^{***}p < 0.001$). See also Figure S2.

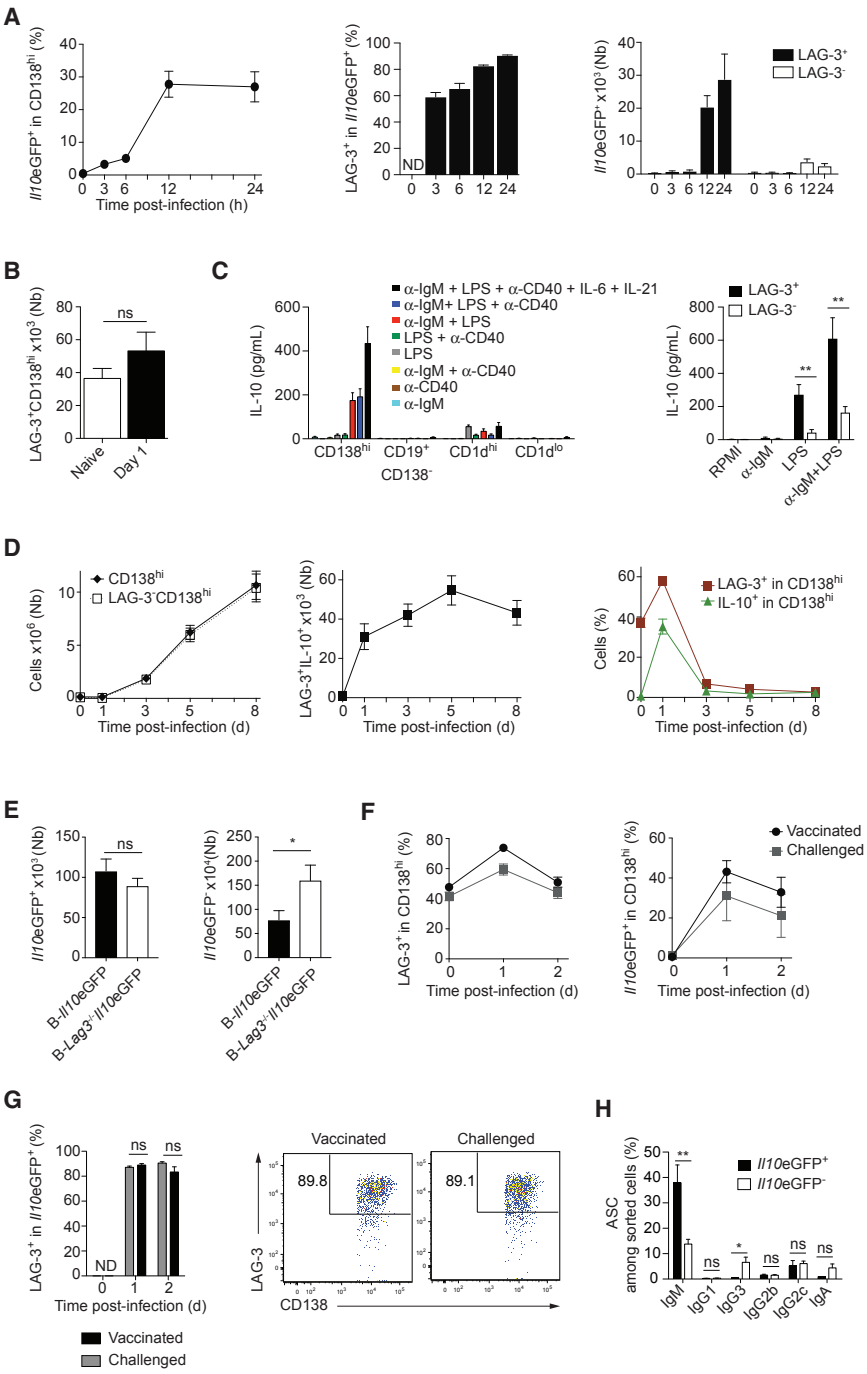

Figure 3. LAG-3$^+$CD138^{hi} Cells Upregulate IL-10 Expression upon Infection

Analyses performed in spleen p.i. (SL7207, 10^7 CFU) or with naive mice.

(A) Kinetics of IL-10 expression in CD138^{hi} cells (left), frequency of LAG-3$^+$ in IL-10$^+$CD138^{hi} cells (middle), numbers of LAG-3$^+$IL-10$^+$CD138^{hi} (LAG-3$^+$) and LAG-3$^-$IL-10$^+$CD138^{hi} (LAG-3$^-$) cells (right) p.i. in *Il10*eGFP mice. Pool of two experiments (n = 6/time point).

(B) Numbers of LAG-3$^+$CD138^{hi} cells in C57BL/6 mice. Pool of four experiments (n = 11/time point).

(C) Isolated cells from naive C57BL/6 mice were stimulated *in vitro* for 18 hr, and IL-10 measured in supernatants. LAG-3$^+$CD138^{hi} and LAG-3$^-$CD138^{hi} cells indicated as LAG-3$^+$ and LAG-3$^-$, respectively. Pool of five experiments.

(D) Numbers of CD138^{hi} and LAG-3$^-$CD138^{hi} cells (left), LAG-3$^+$IL-10$^+$CD138^{hi} cells (middle), frequency of LAG-3$^+$ (red line) or IL-10$^+$ (green line) cells in CD138^{hi} cells (right) p.i. in *Il10*eGFP mice. Pool of 4 experiments; at least 12 mice per group.

(E) Numbers of IL-10$^+$CD138^{hi} and IL-10$^-$CD138^{hi} cells at day 3 p.i. in B-*Il10*eGFP and B-*Lag3*$^{-/-}$*Il10*eGFP chimeric mice.

(F) *Il10*eGFP mice were vaccinated and challenged 90 days later (vaccinated), along with age-matched naive *Il10*eGFP mice (challenged). Frequencies of LAG-3$^+$ in CD138^{hi} cells (left), and of IL-10$^+$ in CD138^{hi} cells (right). Pool of two experiments; at least six mice per group.

(G) *Il10*eGFP mice treated as in (F) and analyzed at day 1 and 2 post-re-challenge. Flow cytometry plots show LAG-3 and CD138 on IL-10$^+$CD138^{hi} cells (right, day 1) with quantifications (left). Pool of two experiments; at least six mice per group.

(H) *Il10*eGFP mice were treated as in (F). Frequency of ASC in indicated plasmocytes on day 1 post-re-challenge by ELISPOT. Pool of two experiments; at least six mice per group.

Data shown are mean ± SEM ($^{ns}p > 0.05$, $^*p < 0.05$, $^{**}p < 0.01$; $^{***}p < 0.001$). See also Figure S3.

(Figure S4F). A hierarchical clustering with all DEGs confirmed the relative proximity of LAG-3$^+$CD138^{hi} cells from naive mice and day 1 p.i. compared to LAG-3$^-$CD138^{hi} cells (Figure 4E). The top DEGs (Tables S1 and S2) included genes coding for IL-10 and the surface proteins LAG-3, CD200, and CXCR3, whose differential expression was also reflected in protein amount (Figures 1 and 2). A Gene Set Enrichment Analysis (MSigDB) of the 648 DEGs in naive mice highlighted cell cycle regulation as the major pathway discriminating the LAG3$^-$ and LAG3$^+$ subsets (Figure S4G). 23 of the 648 DEGs were also differentially methylated between LAG-3$^+$CD138^{hi} and LAG-3$^-$CD138^{hi} cells, including *Il10*, *Bcl2*, *Zfp36l1*, *Irf8*, and other B cell regulators (Figure 4F). This argues for an epigenetically primed control of their expression.

We finally focused on transcription regulators differentially expressed in higher (or lower) amount on both day 0 and 1 p.i. in LAG-3$^+$CD138^{hi} cells as compared to LAG-3$^-$CD138^{hi} cells. We identified 22 factors (including transcription factors and co-factors, gene expression regulators, and general DNA binding proteins) with higher expression in LAG-3$^+$CD138^{hi} cells and 8 factors with higher expression in LAG-3$^-$CD138^{hi} cells (Figure 4G). LAG-3$^+$CD138^{hi} cells showed a higher expression of *Klf4*, *Bhlhe40*, and *Bmyc* that are involved in the inhibition of proliferation, and of *Hes1* that indicates higher Notch signaling activity. They also displayed a higher expression of *Fos*, *Junb*, *Egr1*, *Egr2*, *Cebpb*, *Irf8*, and *Satb1* (Figures 4G and 4H), i.e.,

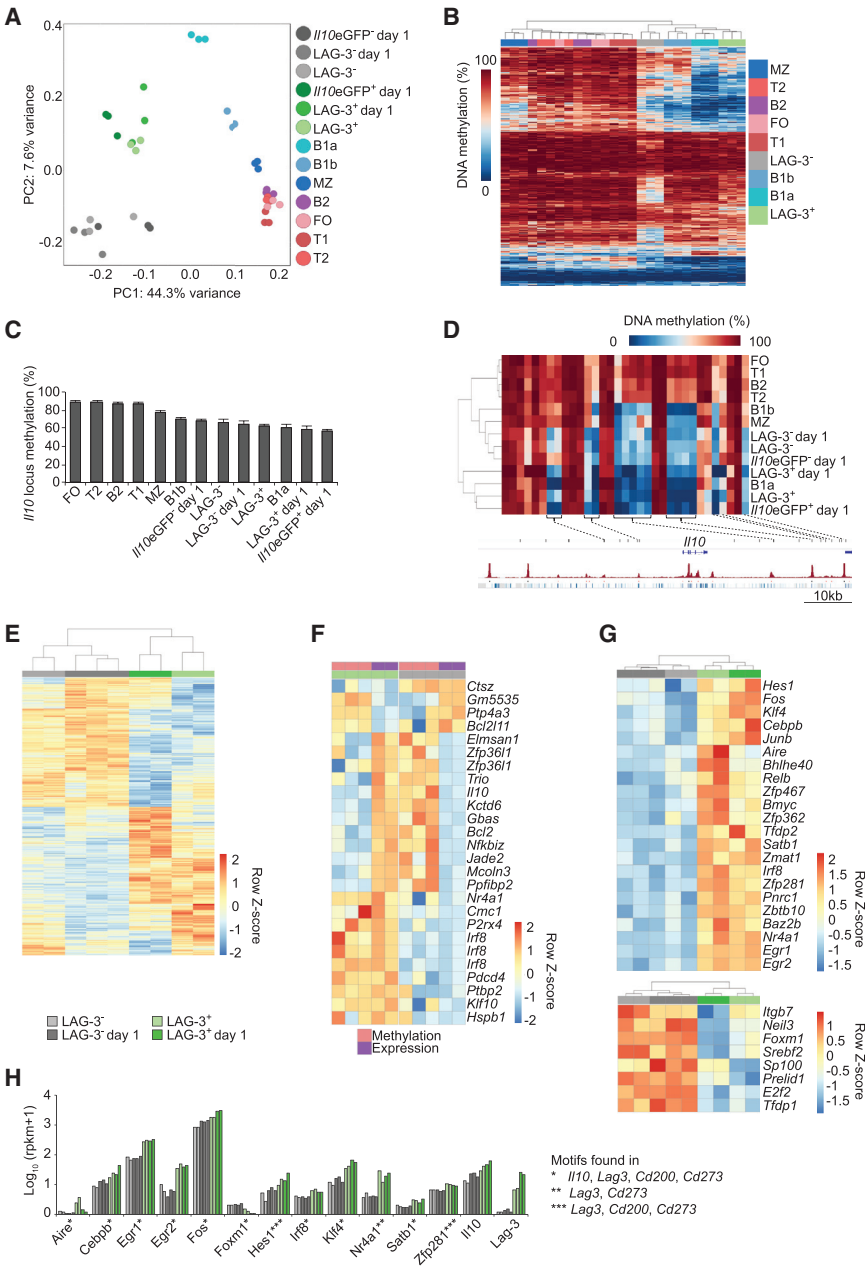

Figure 4. Molecular Characterization of LAG-3$^+$CD138^{hi} Cells

(A) Unsupervised PCA of genome-wide DNA methylation data of cells from C57BL/6 mice.

(B) Methylation of the CpG found in the 469 DMR distinguishing LAG-3$^+$CD138^{hi} cells and LAG-3$^-$CD138^{hi} cells.

(C) DNA methylation of *Il10* locus (mean ± SEM).

(D) Methylation for covered CpG in the *Il10* locus. Coverage weighted average methylation of three replicates is represented. The positions of selected CpG are indicated by vertical black bars, with the *Il10* gene depicted. ENCODE DNase I data are in red for splenic CD43$^-$ B cells. PhastCons Vert30 conservation scores are in blue.

(E) mRNA expression for the 3,631 DEGs that distinguish LAG-3$^+$CD138^{hi} and LAG-3$^-$CD138^{hi} cells on day 0 and 1 p.i. (see Figure S4F).

(F) mRNA expression and local DNA methylation for genes both differentially expressed and methylated between LAG-3$^+$CD138^{hi} and LAG-3$^-$CD138^{hi} cells from naive mice.

(G) Transcription regulators expressed at higher (top) or lower (bottom) amounts on both day 0 and 1 p.i. in LAG-3$^+$CD138^{hi} compared to LAG-3$^-$CD138^{hi} cells.

(H) Expression of transcription regulators differentially expressed between LAG-3$^+$CD138^{hi} cells and LAG-3$^-$CD138^{hi} cells (see G) with predicted binding motif in either the *Il10*, *Lag3*, *Cd200*, or *Cd273* loci.

Row z-scores for expression are based on $\log_{10}$(rpkm+1), and for DNA methylation on DNA methylation frequency (%).

Samples were from naive mice (A, C, D, E, G, H) except where indicated. See also Figure S4.

genes coding for factors for which we found predicted binding sites in the *Il10*, *Lag3*, *Cd200*, and *Cd273* (PD-L2) loci (Figure 4H). FOS, JUN-B, and EGR-2 drive IL-10 expression in other immune cells (Iwasaki et al., 2013; Wang et al., 2005; Yoshida et al., 2012). EGR2 was also important in CD4$^+$ T cells for LAG-3 expression, BLIMP-1-mediated induction of IL-10, and their regulatory activity (Iwasaki et al., 2013). The reduced expression of *Foxm1* in LAG-3$^+$CD138^{hi} cells (Figures 4G and 4H) might be linked to two effects: their lack of proliferation (Chen et al., 2013) and the control of *Il10* transcription since Foxm1 binding sites were predicted in this locus (Figure 4H).

We conclude that LAG-3$^+$CD138^{hi} cells exhibit a distinct transcriptome, partially linked to epigenetic changes, keeping them in a quiescent state primed for IL-10 expression. This molecular program could explain why only this subset of plasmocytes expresses IL-10 and other immune checkpoint receptor molecules.

BCR Repertoire and Developmental Origin of LAG-3$^+$CD138^{hi} Cells

The differentiation of B cells into plasma cells requires the engagement of their BCR by antigen. Our observation that LAG-3$^+$CD138^{hi} cells develop independently of the microbiota prompted us to examine whether they express a particular BCR repertoire.

Single-cell analysis of their IgH and Igk revealed that LAG-3$^+$CD138^{hi} cells and IL-10$^+$CD138^{hi} cells displayed a lower utilization of IgH VH1-81 and a higher usage of VH7, VH10, and VH11 segments compared to LAG-3$^-$CD138^{hi} cells and IL-10$^-$CD138^{hi} cells (Figures 5A and S5A). The majority of VH11$^+$ IgH were associated with a Vk14.126$^+$ (formerly Vk9) Igk (Figure 5B), forming a combination typical of B1a cells (Hardy et al., 2004). Flow cytometry analyses confirmed the presence of a VH11$^+$Vk14.126$^+$ BCRs on splenic LAG-3$^+$CD138^{hi} cells and IL-10$^+$CD138^{hi} cells but not on LAG-3$^-$CD138^{hi} cells or IL-10$^-$CD138^{hi} cells (Figures 5C and S5B). Of note, the BM from naive mice contained IL-10$^+$CD138^{hi} cells (Figure 5D) enriched

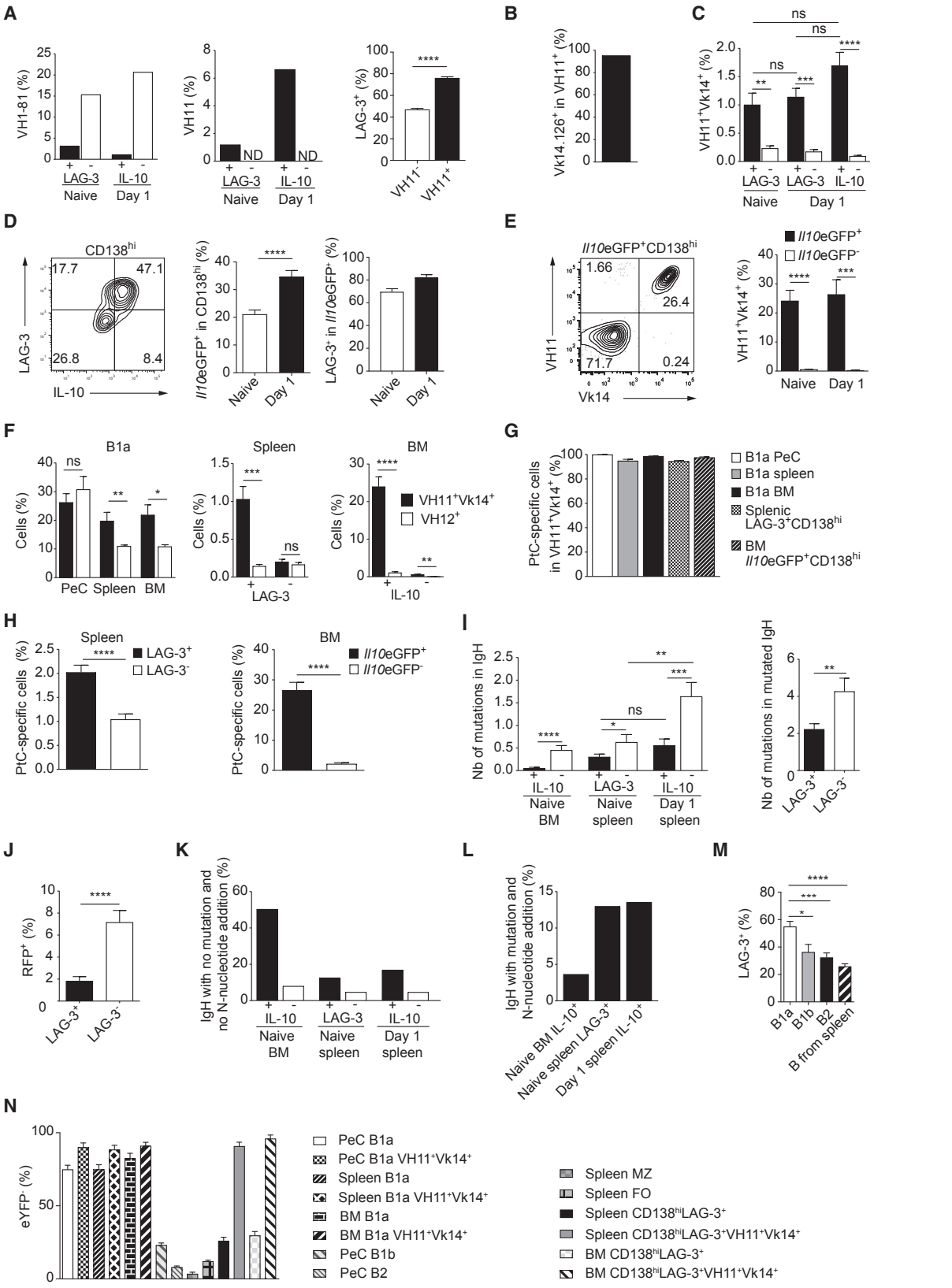

(legend on next page)

in VH11$^+$Vk14.126$^+$ cells (Figure 5E). Thus, some LAG-3$^+$CD138^{hi} and IL-10$^+$CD138^{hi} cells carry a VH11$^+$Vk14.126$^+$ BCRs typical of B1a cells (Figures S5C and S5D). However, the other VH segment classically associated with B1a cells, namely VH12, was not found in spleen LAG-3$^+$CD138^{hi} cells, and only on about 1% of BM IL-10$^+$CD138^{hi} cells (Figure 5F). The VH11$^+$ IgH from LAG-3$^+$CD138^{hi} and IL-10$^+$CD138^{hi} cells had few mutations as well as N-additions, and a large proportion contained the CDR3 characteristic of the anti-phosphatidylcholine (PtC) response (Figures S5E and S5F). Accordingly, nearly all VH11$^+$Vk14.126$^+$ cells displayed reactivity against PtC (Figure 5G), and about 2% of splenic LAG-3$^+$CD138^{hi} cells as well as 26% of BM IL-10$^+$CD138^{hi} cells in naive mice reacted toward this particular antigen (Figure 5H). In BM, more than 80% of PtC-reactive CD138^{hi} cells expressed IL-10 (Figure S5G). Taken together, these data strongly suggest that VH11$^+$Vk14.126$^+$ LAG-3$^+$CD138^{hi} spleen and BM cells derive from B1a cells. Some LAG-3$^+$CD138^{hi} cells expressing other BCR might also derive from B1a cells because LAG-3$^+$CD138^{hi} and IL-10$^+$CD138^{hi} cells had overall fewer IgH somatic mutations than LAG-3$^-$CD138^{hi} and IL-10$^-$CD138^{hi} cells (Figure 5I). This correlated with a lower AID fate-mapping marking of LAG-3$^+$CD138^{hi} cells (Figure 5J). Furthermore, a higher proportion of IgH from LAG-3$^+$CD138^{hi} and IL-10$^+$CD138^{hi} lacked both somatic mutation and N-addition as compared to LAG-3$^-$CD138^{hi} and IL-10$^-$CD138^{hi} cells (Figure 5K). Nonetheless, some LAG-3$^+$CD138^{hi} and IL-10$^+$CD138^{hi} cells expressed IgH sequences with mutations and N-additions (Figure 5L), suggesting an additional origin for LAG-3$^+$CD138^{hi} cells.

To evaluate the capacity of various B cell subsets to generate LAG-3$^+$CD138^{hi} cells, we adoptively transferred B1a, B1b, and B2 cells from peritoneal cavity (PeC) as well as splenic B cells into *Rag2*$^{-/-}$ mice (Figure 5M). The analysis of the recipient mice confirmed that several B cell subsets could give rise to LAG-3$^+$CD138^{hi} cells, as observed also upon culture of B cell subsets *in vitro* (Figure S5H). Marginal zone B cells were not a non-redundant source of LAG-3$^+$CD138^{hi} cells *in vivo* since mice that lacked marginal zone B cells due to a B cell-restricted deficiency in NOTCH2 (Saito et al., 2003) displayed normal frequency of LAG-3$^+$CD138^{hi} cells (Figure S5I) despite their globally reduced numbers of splenic plasmocytes (data not shown). To further delineate the origin of LAG-3$^+$CD138^{hi} cells in a physiological context, we next developed a fate mapping system using the fact that B1a cells poorly expressed CD21 compared to other B cell susbsets, and crossed *Cd21*-cre mice to ROSA-STOP-eYFP reporter mice. In *Cd21*-cre-ROSA-STOP-eYFP mice, most B1a cells were eYFP$^-$ in PeC, spleen, and BM, which was even more apparent when focusing on the VH11$^+$Vk14$^+$ fraction of B1a cells (Figure 5N). In contrast, B1b and B2 cells from PeC as well as follicular and marginal zone B cells from spleen were mostly eYFP$^+$ (Figure 5N). The LAG-3$^+$CD138^{hi} cell subset contained an intermediate frequency of eYFP$^-$ cells, underlining their heterogeneous origin. Importantly, the LAG-3$^+$CD138^{hi} cells that carried a VH11$^+$Vk14$^+$ BCR were largely eYFP$^-$, indicating that eYFP$^-$ B1a cells did not switch-on eYFP expression during their differentiation into LAG-3$^+$CD138^{hi} cells (Figure 5N).

We conclude that LAG-3$^+$CD138^{hi} cells develop from several B cell subsets via a mechanism involving the BCR since they have a distinct BCR repertoire.

Roles of BCR and TLR in LAG-3$^+$CD138^{hi} Plasma Cell Development and Function

We next examined how the BCR influenced the accumulation of LAG-3$^+$CD138^{hi} cells in naive mice and their upregulation of IL-10 after challenge.

The Bruton tyrosine kinase (Btk) is essential for BCR signaling (Corneth et al., 2016). *Btk*$^{-/-}$ mice showed a developmental defect in B1a cells but not in B1b cells and marginal zone B cells (Figure 6A). They also displayed reduced frequencies and numbers of LAG-3$^+$CD138^{hi} cells (Figure 6A). We next assessed the effect of the BCR co-receptors CD19 and CD72 for the generation of LAG-3$^+$CD138^{hi} cells. We also studied mice genetically deficient in proteins involved in antigen presentation

Figure 5. BCR Repertoire of LAG-3$^+$ and IL-10$^+$ Plasmocytes

(A) Frequency of *Igh* containing VH1-81 (left) or VH11 (middle) in spleen LAG-3$^+$CD138^{hi} (n = 253), LAG-3$^-$CD138^{hi} (n = 150), *Il10*eGFP$^+$CD138^{hi} (n = 181), and *Il10*eGFP$^-$CD138^{hi} (n = 121) cells on day 0 and day 1 p.i. (SL7207; 10^7 CFU). Frequency of LAG-3$^+$ in VH11$^+$CD138^{hi} and VH11$^-$CD138^{hi} spleen cells of naive mice (n = 12) (right).

(B) Frequency of Vk14.126$^+$ cells in VH11$^+$ cells for spleen and BM cells described in Figure S5A.

(C) Frequency of VH11$^+$Vk14.126$^+$ cells by flow cytometry. Pool of two experiments (6–7 mice/group/time point).

(D) Flow cytometry plot of LAG-3 versus *Il10*eGFP in CD138^{hi} BM cells at day 1, and quantifications. Pool of four experiments (n = 12–17/time point).

(E) Flow cytometry plot and frequency of VH11$^+$Vk14.126$^+$ cells in IL-10$^+$CD138^{hi} cells in BM of *Il10*eGFP mice. Pool of two experiments (n = 6–7/time point).

(F) Frequency of VH11$^+$Vk14.126$^+$ and VH12$^+$ cells in B1a cells from indicated tissues (left), spleen LAG-3$^+$ and LAG-3$^-$ (middle), and BM IL-10$^+$ and IL-10$^-$ (right) plasmocytes from naive mice. Pool of two experiments (n = 7).

(G) Frequency of PtC-reactive cells in VH11$^+$Vk14.126$^+$ cells for indicated cells from naive mice. Pool of two experiments (n = 7).

(H) Frequency of PtC-reactive cells in indicated plasmocytes from naive mice. Pool of four experiments (n = 12).

(I) Mutations in IgH sequences (naive BM *Il10*eGFP$^+$CD138^{hi}, n = 165; *Il10*eGFP$^-$CD138^{hi}, n = 151; naive spleen LAG-3$^+$CD138^{hi}, n = 231; LAG-3$^-$CD138^{hi}, n = 129; day 1 spleen *Il10*eGFP$^+$CD138^{hi}, n = 155; *Il10*eGFP$^-$CD138^{hi}, n = 108) (left). Number of somatic mutations per sequence for mutated IgH (LAG-3$^+$CD138^{hi} cells, n = 31; LAG-3$^-$CD138^{hi} cells, n = 19) (right).

(J) *Aicda*-cre-ERT2-ROSA-STOP-RFP mice were treated with tamoxifen and analyzed 15 days after the last treatment. Frequency of RFP$^+$ cells in LAG-3$^+$CD138^{hi} and LAG-3$^-$CD138^{hi} spleen cells. Pool of five experiments (n = 14).

(K) Frequency of IgH sequences (as in I) having no mutation and no N-nucleotide addition.

(L) Frequency of IgH sequences (as in I) with mutation and N-nucleotide addition.

(M) Frequency of LAG-3$^+$ in spleen CD138^{hi} cells 3 weeks after transfer of indicated cell fractions into *Rag2*$^{-/-}$ mice. Pool of three experiments (n = 6–7/group).

(N) Frequency of eYFP$^-$ cells in indicated cells of naive *Cd21*-cre-ROSA-STOP-eYFP mice. Pool of three experiments (n = 6).

Groups were compared using two-tailed unpaired t test with Welch's correction in case of inequal variances (C–I) or using Mann-Whitney test (M). Data are mean ± SEM ($^{ns}p > 0.05$, $^*p < 0.05$, $^{**}p < 0.01$; $^{***}p < 0.001$, $^{****}p < 0.0001$). See also Figure S5.

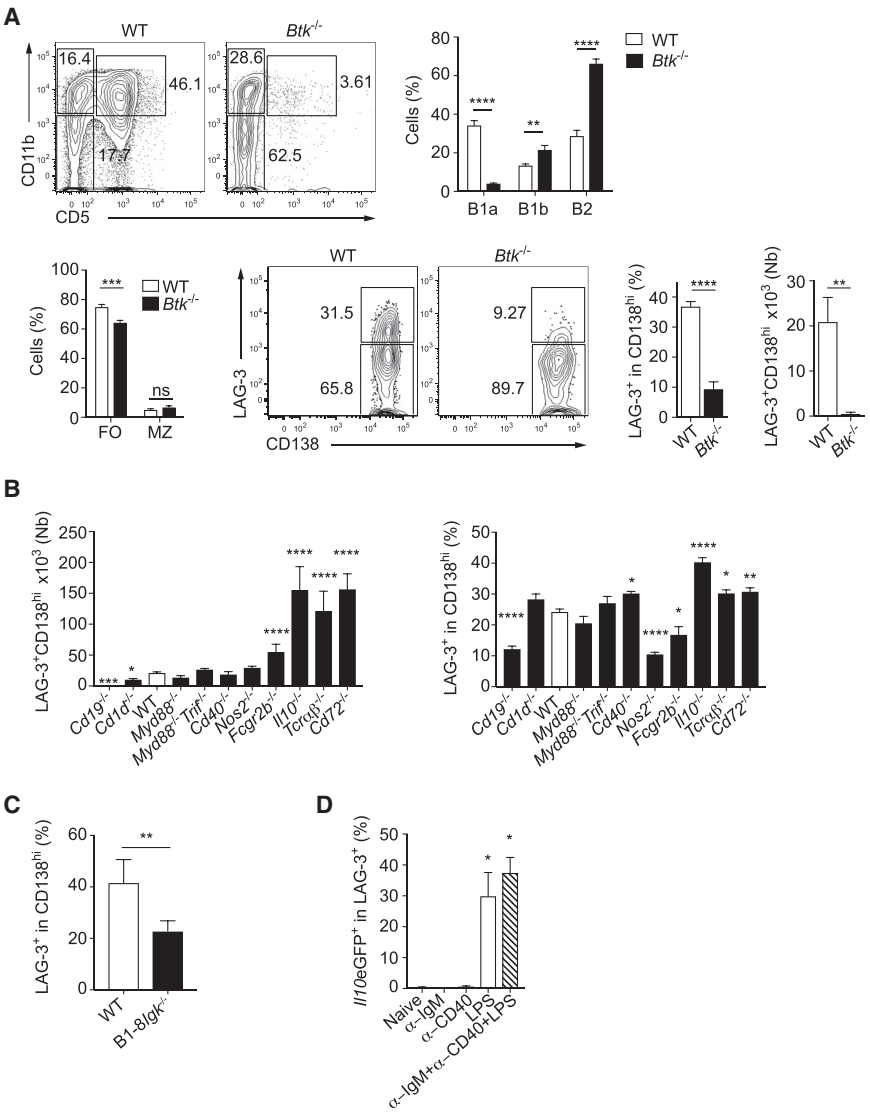

Figure 6. Molecules Implicated in the Homeostasis of LAG-3$^+$CD138^{hi} Cells

(A) Flow cytometry plots and quantification of indicated cells in PeC (top) and spleen (bottom) of naive *Btk*$^{-/-}$ mice and littermate controls. Pool of two experiments (n = 6).

(B) Numbers and frequencies of LAG-3$^+$CD138^{hi} cells in CD138^{hi} plasmocytes in spleen of naive C57BL/6 (n = 40), *Cd19*$^{-/-}$ (n = 5), *Il10*$^{-/-}$ (n = 8), *Tcrab*$^{-/-}$ (n = 7), *Cd72*$^{-/-}$ (n = 10), *Cd1d*$^{-/-}$ (n = 6), *Myd88*$^{-/-}$ (n = 10), *Myd88*$^{-/-}$*Trif*$^{-/-}$ (n = 12), *Cd40*$^{-/-}$ (n = 6), *Nos2*$^{-/-}$ (n = 10), and *Fcgr2b*$^{-/-}$ (n = 5) mice.

(C) Frequencies of LAG-3$^+$ in spleen CD138^{hi} cells of B1-8i*Igk*$^{-/-}$ and WT mice. Pool of two experiments (n = 4–5).

(D) Frequency of IL-10 in spleen LAG-3$^+$CD138^{hi} of *Il10*eGFP mice 24 hr after i.v. injection of indicated reagents. Pool of three experiments (n = 6).

Data show mean ± SEM (^{ns}p > 0.05, *p < 0.05, **p < 0.01; ***p < 0.001, ****p < 0.0001). See also Figure S6.

(CD1d), innate immune signaling (MyD88 and TRIF), T cell:B cell interaction (CD40, T cell receptor for antigen), and inflammation (NOS2, IL-10) (Figure 6B). LAG-3$^+$CD138^{hi} cells were present in lower amounts in mice deficient for CD19, which is a positive regulator of BCR signaling, and in higher numbers in mice lacking CD72, which is an inhibitory BCR co-receptor. In contrast, they were normally present in *Myd88*$^{-/-}$*Trif*$^{-/-}$ mice, which lacked TLR signaling. Mice deficient in CD40 or αβTCR-expressing T cells also generated these cells normally. LAG-3$^+$CD138^{hi} cells can therefore develop independently of canonical T cell:B cell interactions and are thus not strictly dependent on a T cell-dependent antigen. The finding that BCR but not TLR signaling contributed to the formation of LAG-3$^+$CD138^{hi} cells led us to assess whether mice with a restricted BCR repertoire had an altered abundance of these plasma cells. Indeed, B1-8i mice carrying a fixed IgH chain on an Igk-deficient background displayed a 2-fold reduction in the frequency of LAG-3$^+$CD138^{hi} cells compared to controls (Figure 6C). Of note, antibodies cloned from LAG-3$^+$CD138^{hi} cells displayed little polyreactivity when tested as recombinant molecules in ELISA (Tiller et al., 2009), unlike those from BM IL-10$^-$IgM$^+$CD138^{hi} cells (Figure S6A). Considering that BCR signaling contributed to the development of LAG-3$^+$CD138^{hi} cells at steady state, we next asked whether such cells could be generated upon immunization with 4-hydroxy-3-nitrophenylacetyl keyhole limpet hemocyanin (NP-KLH), NP-Ficoll, or NP-LPS i.e., classical T cell-dependent, T cell-independent type II, and T cell-independent type I antigens, respectively (Figure S6B). These immunizations induced NP-reactive LAG-3$^-$CD138^{hi} cells, but not NP-reactive LAG-3$^+$CD138^{hi} cells. We conclude that LAG-3$^+$CD138^{hi} cells develop from B cells at steady state upon a particular form of BCR engagement that is not recapitulated by these immunizations.

We next asked whether BCR or other signals controlled the upregulation of IL-10 expression in LAG-3$^+$CD138^{hi} cells after challenge. To this end, *Il10*eGFP mice were injected intravenously with anti-BCR, anti-CD40, or LPS, alone or in combination (Figure 6D). The administration of anti-BCR or anti-CD40 had no effect on IL-10 expression, yet LPS induced a strong upregulation of IL-10 in LAG-3$^+$CD138^{hi} cells. These results demonstrated that IL-10 expression was induced in a polyclonal manner in LAG-3$^+$CD138^{hi} cells upon TLR4 stimulation. This was in agreement with the fact that LAG-3$^+$CD138^{hi} cells from naive mice, as well as of LAG-3$^+$CD138^{hi} cells and IL-10$^+$CD138^{hi} cells from day 1 p.i., had comparable frequencies of VH11$^+$Vk14$^+$ cells (Figure 5C), suggesting that IL-10 was induced in LAG-3$^+$CD138^{hi} cells in a polyclonal manner.

We conclude that the development of LAG-3$^+$CD138^{hi} cells is controlled by the BCR and independent of TLR signaling as well

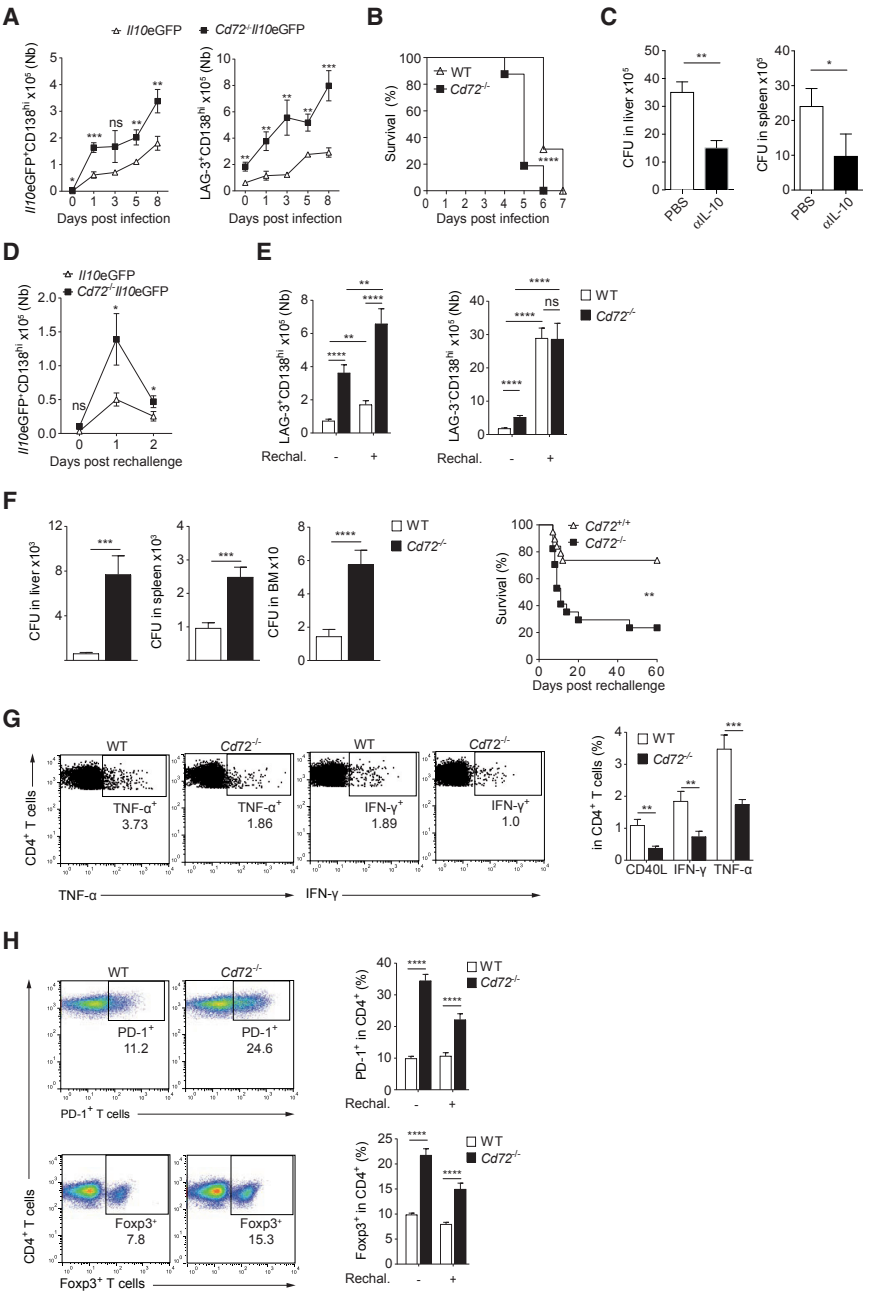

Figure 7. CD72 Deficiency Enhances Susceptibility to *Salmonella*

(A) Numbers of indicated spleen cells in *Il10*eGFP and *Cd72*$^{-/-}$*Il10*eGFP mice p.i. (SL7207, 10^7 CFU). Pool of three experiments (n = 9–12/time point/group).

(B) Survival of *Cd72*$^{-/-}$ (n = 16) and controls (n = 16) after infection (SL1344, 100 CFU). Pool of two experiments.

(C) CFU on day 3 p.i. (SL7207, 10^7 CFU) of anti-IL10 plus anti-IL10R-treated and control *Cd72*$^{-/-}$ mice. Pool of two experiments (n = 6–10/group).

(D) Mice were vaccinated (SL7207, 10^6 CFU) and re-challenged on day 90 (SL7207, 10^7 CFU). Numbers of cells in spleen after re-challenge. Pool of three experiments (n = 9/group/time point).

(E) Mice were vaccinated (SL7207, 10^6 CFU), re-challenged on day 90 (SL7207, 10^6 CFU), and analyzed 5 days later with (+) or without (–) re-challenge. Pool of four experiments (n = 15–18/group/time point).

(F) CFU on day 5 post-re-challenge for mice shown in (E) (left). Survival of *Cd72*$^{-/-}$ (n = 17) and littermate control (n = 19) mice vaccinated (SL7207, 10^6 CFU) and re-challenged 90 days later (SL1344, 100 CFU). Pool of two experiments (right).

(G) *Cd72*$^{-/-}$ and WT mice were vaccinated (SL7207, 10^6 CFU), and BM analyzed on day 90. Flow cytometry plot (left) and quantifications (right) for CD40L, TNF-α, and IFN-γ expression in *Salmonella*-reactive memory CD4$^+$ T cells. Pool of three experiments (n = 12).

(H) Flow cytometry plots showing PD-1 and FOXP-3 in spleen CD4$^+$ T cells of mice treated as in (E) and analyzed on day 0 and 5 post-rechallenge. Pool of three experiments (n = 12/group).

Groups were compared using two-tailed unpaired t test ($^{ns}p > 0.05$, $^*p < 0.05$, $^{**}p < 0.01$; $^{***}p < 0.001$, $^{****}p < 0.0001$). Survival curves were compared using Wilcoxon test, $^{**}p < 0.01$, $^{****}p < 0.0001$. Data show mean ± SEM. See also Figure S7.

as T cell help, while their upregulation of IL-10 after challenge is determined by TLR signaling.

Elevated Abundance of LAG-3$^+$CD138^{hi} Cells Correlates with Impaired Immunity against *Salmonella*

An ablation of IL-10 production by CD138^{hi} plasmocytes increased host defense to *Salmonella* (Neves et al., 2010). Here, we sought to determine how an increased abundance of LAG-3$^+$CD138^{hi} cells affected host resistance to this infection using *Cd72*$^{-/-}$ mice.

Cd72$^{-/-}$ mice had an increased number of LAG-3$^+$CD138^{hi} cells, while other B cell subsets did not display any major defect (Figure S7A). The increased accumulation of LAG-3$^+$CD138^{hi} cells in *Cd72*$^{-/-}$ mutants was confirmed with littermate mice (Figure S7A). After infection, *Cd72*$^{-/-}$ mice displayed an increased accumulation of IL-10$^+$CD138^{hi} and LAG-3$^+$CD138^{hi} cells (Figures 7A and S7B), an impaired control of the infection (Figure S7C), and a reduced survival (Figure 7B) compared to controls. The CD72 deficiency had no effect in B cell-deficient mice, confirming that the observed differences were due to the lack of *Cd72* in B cells (Figure S7D). To validate the inhibitory impact of IL-10 on host defense in *Cd72*$^{-/-}$ mice, mice were treated intravenously with a combination of anti-IL-10 and anti-IL-10 receptor. This significantly improved the control of the bacteria (Figure 7C). Since LAG-3$^+$CD138^{hi} cells are the major source of IL-10 after infection, this supports the notion that LAG-3$^+$CD138^{hi} cells inhibit host defense through IL-10 provision.

Finally, we investigated how CD72 deficiency affected the host response to secondary infection. *Il10*eGFP and *Cd72*$^{-/-}$*Il10*eGFP

mice were vaccinated and later challenged with *Salmonella*. Mice lacking *Cd72* displayed a higher accumulation of IL-10^{+}CD138^{hi} cells and LAG-3^{+}CD138^{hi} cells upon re-challenge, while LAG-3^{-}CD138^{hi} and total CD138^{hi} cells were present in comparable numbers in the two groups of mice (Figures 7D, 7E, and S7E). Consistently, CD72 deficiency led to higher bacterial load and reduced survival (Figure 7F), compromising vaccine efficacy. Memory T helper 1 (Th1) cells play a major role in vaccine-induced protection against *Salmonella*. In vaccinated *Cd72*$^{-/-}$ mice, numbers of memory *Salmonella*-reactive Th1 CD4^{+} T cells in the BM were reduced (Figures 7G and S7F), and accumulation of exhausted PD-1^{+}CD4^{+} T cells, PD-1^{+}CD8^{+} T cells, and regulatory Foxp3^{+}CD4^{+} T cells were increased (Figures 7H and S7G).

These data demonstrate that in the absence of CD72, a higher accumulation of LAG-3^{+}CD138^{hi} plasma cells is associated with impaired immunity to *Salmonella*.

DISCUSSION

This study demonstrates the existence of natural regulatory plasma cells, which are the major source of IL-10 early after infection with *Salmonella*.

An unexpected finding was that the cells expressing IL-10 were not reactive plasmablasts but instead resident plasma cells. Upon activation, B cells successively generated antibody-secreting plasmablasts that proliferated and then plasma cells that did not divide and expressed higher amounts of the transcription factor BLIMP-1. LAG-3^{+}CD138^{hi} cells were non-proliferating and expressed higher amounts of BLIMP-1 than LAG-3^{-}CD138^{hi} cells, thus qualifying as *bone fide* plasma cells. Their non-dividing status correlated with the lack of expression of factors necessary for cell division including the transferrin receptor CD71 and the transcriptional regulator Foxm1, as well as the increased expression of the cell proliferation inhibitors *Egr2*, *Zfp36l1*, *Pdcd4*, *Klf4*, and *Bhlhe40*. KLF4 is absent in plasmablasts generated *in vitro* but is expressed in long-lived BM plasma cells (Schoenhals et al., 2016). LAG-3^{+}CD138^{hi} cells thus display a profile of mature plasma cells, while retaining the capacity to respond to external stimuli, in particular TLR, via the production of IL-10.

LAG-3^{+}CD138^{hi} plasma cells expressed several immune checkpoint receptors implicated in the negative regulation of immunity such as LAG-3, PD-L1, PD-L2, and CD200. LAG-3 is a co-inhibitory receptor related to CD4 and implicated in the down-modulation of T cell immunity. The co-expression of several inhibitory molecules is important because these molecules usually act synergistically, so that their combined blockade achieves greater effect than the neutralization of single molecules. Blockade of LAG-3 and PD-L1 augments immunity toward *Plasmodium falciparum* by amplifying T cell activation and antibody production (Butler et al., 2011). Here, we found that LAG-3 on plasma cells did not influence their IL-10 expression, but inhibited the accumulation of IL-10^{-}CD138^{hi} cells, which were LAG-3^{-}, early after infection. The suppressive function of LAG-3^{+}CD138^{hi} cells therefore extends beyond IL-10 production, suggesting a more global role in immune regulation.

LAG-3^{+}CD138^{hi} cells developed from several B cell subsets in a BCR-dependent manner. Their preserved accumulation in germ-free mice suggests that they are selected on self-antigens. Our study has not identified the antigens involved in the generation of LAG-3^{+}CD138^{hi} cells. Since these cells increased with age, which has also been associated with an accumulation of damaged cells (Baker et al., 2016), it is tempting to speculate that LAG-3^{+}CD138^{hi} cells react toward antigens released by damaged cells. This hypothesis is consistent with the recognition by natural IgM of senescent cells (Frescas et al., 2017) and by natural antibodies binding PtC of apoptotic cells (Shaw et al., 2000). LAG-3^{+}CD138^{hi} cells may thus provide a feedback mechanism, which senses the number of damaged cells and proportionally downregulates the activation of immunity to limit additional and potentially excessive immunopathology when an immune stimulus arises. Mice lacking the BCR inhibitory co-receptor CD72 had an increased abundance of LAG-3^{+}CD138^{hi} cells and an impaired capacity to control *Salmonella* infection. The induction of IL-10 in LAG-3^{+}CD138^{hi} cells was primarily controlled by TLR. We cannot, however, exclude that BCR signaling played a role in IL-10 production, even if it was not the major switch for IL-10 expression. For instance, it might contribute to the transcription of *Il10* in LAG-3^{+}CD138^{hi} cells at steady state in naive mice and synergize with TLR to upregulate IL-10 expression after challenge. It is indeed possible that these cells express BCR that recognize endogenous antigens already available at steady state and persisting during challenge.

In conclusion, natural regulatory plasma cells can rapidly provide a first layer of B cell-mediated immune regulation in response to TLR signals. They might subsequently be complemented by other subsets of suppressive B cells and plasma cells induced in an antigen-specific manner.

STAR★METHODS

Detailed methods are provided in the online version of this paper and include the following:

- KEY RESOURCES TABLE
- CONTACT FOR REAGENT AND RESOURCE SHARING
- EXPERIMENTAL MODEL AND SUBJECT DETAILS
  - Mice
- METHOD DETAILS
  - Bacterial infection
  - Tamoxifen administration
  - Immunization and treatment with agonists of BCR, CD40, TLR4
  - Isolation of plasmocytes and B cells
  - B cell stimulation and cytokine production measurement
  - Transmission Electron Microscopy
  - Gene array hybridization
  - Library preparation for methylation analysis of plasmocytes and B cell subsets
  - Library preparation for mRNA Seq
  - Analysis of mRNA expression by B cells and plasmocytes
  - Ig gene amplification from single cells
  - Cloning of mouse Ig genes into expression vectors
  - Expression of recombinant immunoglobulin
  - Detection of antibody reactivity by ELISAs
  - Cell staining for flow cytometry

SUPPLEMENTAL INFORMATION

Supplemental Information includes eight figures and two tables and can be found with this article online at https://doi.org/10.1016/j.immuni.2018.06.007.

ACKNOWLEDGMENTS

We thank J. Kirsch, H. Schliemann, the Regine von Ramin Laboratory (DRFZ), and A.B. Koehler (Max Planck Institute of Infection Biology) for technical help, K. Rajewsky (MDC, Berlin) for VH12, K. Hayakawa (Fox Chase Cancer Center, USA) for VH11 and Vk14 antibodies, H. Wardemann (DKFZ, Heidelberg) for Ig expression plasmids, S. Nutt (WEHI, Australia) for *Prdm1*eGFP mice, H.J. Fehling (Ulm) for ROSA-STOP-tdRFP mice, and D. Vignali, St. Jude Children's Research Hospital, and IGBMC for *Lag3*$^{-/-}$ mice. S.F. lab is supported by ERC PREG-LAB 647696, AXA Chair Translational Immunology, Agence Nationale de la Recherche (ANR-16-CE18-0007-01), Chair of Excellence (Université Sorbonne Paris Cité), and Infect-ERA project ABIR (031A403), Deutsche Forschungsgemeinschaft (TRR130, FI 1238/1-2). T.T. is supported by JSPS KAKENHI 26293062 and 17H05790 grants. J.W. was supported by the German Ministry for Education and Research BMBF through the grant 01KU1216F (DEEP). V.D.D. received a 4-year PhD fellowship from the Vietnam Ministry of Education and Training (Projects 322 and 911).

AUTHOR CONTRIBUTIONS

A.C.L., V.D.D., V.L., A.W., J.J., J.P., Q.S., J.T., A.B., V.F., I.S., U.S., S.R., L.J., P.B., T.T., T.A., A.H., T.D., U.Z.-S., A.F.V., K.D., G.L., S.K., C.G., J.-C.W., C.-A.R., S.H.E.K., J.W., and S.F. performed experiments and contributed to project development and writing of the manuscript.

DECLARATION OF INTERESTS

The authors declare no competing interests.

Received: October 11, 2017
Revised: April 18, 2018
Accepted: June 15, 2018
Published: July 10, 2018

REFERENCES

Akalin, A., Kormaksson, M., Li, S., Garrett-Bakelman, F.E., Figueroa, M.E., Melnick, A., and Mason, C.E. (2012). methylKit: a comprehensive R package for the analysis of genome-wide DNA methylation profiles. Genome Biol. *13*, R87.

Baker, D.J., Childs, B.G., Durik, M., Wijers, M.E., Sieben, C.J., Zhong, J., Saltness, R.A., Jeganathan, K.B., Verzosa, G.C., Pezeshki, A., et al. (2016). Naturally occurring p16(Ink4a)-positive cells shorten healthy lifespan. Nature *530*, 184–189.

Blair, P.A., Chavez-Rueda, K.A., Evans, J.G., Shlomchik, M.J., Eddaoudi, A., Isenberg, D.A., Ehrenstein, M.R., and Mauri, C. (2009). Selective targeting of B cells with agonistic anti-CD40 is an efficacious strategy for the generation of induced regulatory T2-like B cells and for the suppression of lupus in MRL/lpr mice. J. Immunol. *182*, 3492–3502.

Butler, N.S., Moebius, J., Pewe, L.L., Traore, B., Doumbo, O.K., Tygrett, L.T., Waldschmidt, T.J., Crompton, P.D., and Harty, J.T. (2011). Therapeutic blockade of PD-L1 and LAG-3 rapidly clears established blood-stage Plasmodium infection. Nat. Immunol. *13*, 188–195.

Chen, X., Müller, G.A., Quaas, M., Fischer, M., Han, N., Stutchbury, B., Sharrocks, A.D., and Engeland, K. (2013). The forkhead transcription factor FOXM1 controls cell cycle-dependent gene expression through an atypical chromatin binding mechanism. Mol. Cell. Biol. *33*, 227–236.

Chen, T.W., Li, H.P., Lee, C.C., Gan, R.C., Huang, P.J., Wu, T.H., Lee, C.Y., Chang, Y.F., and Tang, P. (2014). ChIPseek, a web-based analysis tool for ChIP data. BMC Genomics *15*, 539.

Corneth, O.B.J., Klein Wolterink, R.G.J., and Hendriks, R.W. (2016). BTK Signaling in B Cell Differentiation and Autoimmunity. Curr. Top. Microbiol. Immunol. *393*, 67–105.

DeLuca, D.S., Levin, J.Z., Sivachenko, A., Fennell, T., Nazaire, M.D., Williams, C., Reich, M., Winckler, W., and Getz, G. (2012). RNA-SeQC: RNA-seq metrics for quality control and process optimization. Bioinformatics *28*, 1530–1532.

Dobin, A., and Gingeras, T.R. (2015). Mapping RNA-seq Reads with STAR. Curr Protoc Bioinformatics *51*, 11 14 11-19.

Durek, P., Nordström, K., Gasparoni, G., Salhab, A., Kressler, C., de Almeida, M., Bassler, K., Ulas, T., Schmidt, F., Xiong, J., et al.; DEEP Consortium (2016). Epigenomic profiling of human CD4^{+} T cells supports a linear differentiation model and highlights molecular regulators of memory development. Immunity *45*, 1148–1161.

Fillatreau, S., Sweenie, C.H., McGeachy, M.J., Gray, D., and Anderton, S.M. (2002). B cells regulate autoimmunity by provision of IL-10. Nat. Immunol. *3*, 944–950.

Frescas, D., Roux, C.M., Aygun-Sunar, S., Gleiberman, A.S., Krasnov, P., Kurnasov, O.V., Strom, E., Virtuoso, L.P., Wrobel, M., Osterman, A.L., et al. (2017). Senescent cells expose and secrete an oxidized form of membrane-bound vimentin as revealed by a natural polyreactive antibody. Proc. Natl. Acad. Sci. USA *114*, E1668–E1677.

Gagliani, N., Magnani, C.F., Huber, S., Gianolini, M.E., Pala, M., Licona-Limon, P., Guo, B., Herbert, D.R., Bulfone, A., Trentini, F., et al. (2013). Coexpression of CD49b and LAG-3 identifies human and mouse T regulatory type 1 cells. Nat. Med. *19*, 739–746.

Gautier, L., Cope, L., Bolstad, B.M., and Irizarry, R.A. (2004). affy–analysis of Affymetrix GeneChip data at the probe level. Bioinformatics *20*, 307–315.

Hardy, R.R., Wei, C.J., and Hayakawa, K. (2004). Selection during development of VH11+ B cells: a model for natural autoantibody-producing CD5+ B cells. Immunol. Rev. *197*, 60–74.

Iwasaki, Y., Fujio, K., Okamura, T., Yanai, A., Sumitomo, S., Shoda, H., Tamura, T., Yoshida, H., Charnay, P., and Yamamoto, K. (2013). Egr-2 transcription factor is required for Blimp-1-mediated IL-10 production in IL-27-stimulated CD4+ T cells. Eur. J. Immunol. *43*, 1063–1073.

Kulis, M., Merkel, A., Heath, S., Queirós, A.C., Schuyler, R.P., Castellano, G., Beekman, R., Raineri, E., Esteve, A., Clot, G., et al. (2015). Whole-genome fingerprint of the DNA methylome during human B cell differentiation. Nat. Genet. *47*, 746–756.

Liao, Y., Smyth, G.K., and Shi, W. (2014). featureCounts: an efficient general purpose program for assigning sequence reads to genomic features. Bioinformatics *30*, 923–930.

Matsumoto, M., Baba, A., Yokota, T., Nishikawa, H., Ohkawa, Y., Kayama, H., Kallies, A., Nutt, S.L., Sakaguchi, S., Takeda, K., et al. (2014). Interleukin-10-producing plasmablasts exert regulatory function in autoimmune inflammation. Immunity *41*, 1040–1051.

McLean, C.Y., Bristor, D., Hiller, M., Clarke, S.L., Schaar, B.T., Lowe, C.B., Wenger, A.M., and Bejerano, G. (2010). GREAT improves functional interpretation of cis-regulatory regions. Nat. Biotechnol. *28*, 495–501.

Miyazaki, T., Dierich, A., Benoist, C., and Mathis, D. (1996). Independent modes of natural killing distinguished in mice lacking Lag3. Science *272*, 405–408.

Neves, P., Lampropoulou, V., Calderon-Gomez, E., Roch, T., Stervbo, U., Shen, P., Kühl, A.A., Loddenkemper, C., Haury, M., Nedospasov, S.A., et al. (2010). Signaling via the MyD88 adaptor protein in B cells suppresses protective immunity during *Salmonella* typhimurium infection. Immunity *33*, 777–790.

Ritchie, M.E., Phipson, B., Wu, D., Hu, Y., Law, C.W., Shi, W., and Smyth, G.K. (2015). limma powers differential expression analyses for RNA-sequencing and microarray studies. Nucleic Acids Res. *43*, e47.

Robinson, M.D., McCarthy, D.J., and Smyth, G.K. (2010). edgeR: a Bioconductor package for differential expression analysis of digital gene expression data. Bioinformatics *26*, 139–140.

Saito, T., Chiba, S., Ichikawa, M., Kunisato, A., Asai, T., Shimizu, K., Yamaguchi, T., Yamamoto, G., Seo, S., Kumano, K., et al. (2003). Notch2 is preferentially expressed in mature B cells and indispensable for marginal zone B lineage development. Immunity *18*, 675–685.

Schoenhals, M., Jourdan, M., Seckinger, A., Pantesco, V., Hose, D., Kassambara, A., Moreaux, J., and Klein, B. (2016). Forced KLF4 expression increases the generation of mature plasma cells and uncovers a network linked with plasma cell stage. Cell Cycle *15*, 1919–1928.

Shalapour, S., Font-Burgada, J., Di Caro, G., Zhong, Z., Sanchez-Lopez, E., Dhar, D., Willimsky, G., Ammirante, M., Strasner, A., Hansel, D.E., et al. (2015). Immunosuppressive plasma cells impede T-cell-dependent immunogenic chemotherapy. Nature *521*, 94–98.

Shaw, P.X., Hörkkö, S., Chang, M.K., Curtiss, L.K., Palinski, W., Silverman, G.J., and Witztum, J.L. (2000). Natural antibodies with the T15 idiotype may act in atherosclerosis, apoptotic clearance, and protective immunity. J. Clin. Invest. *105*, 1731–1740.

Shen, P., and Fillatreau, S. (2015). Antibody-independent functions of B cells: a focus on cytokines. Nat. Rev. Immunol. *15*, 441–451.

Shen, P., Roch, T., Lampropoulou, V., O'Connor, R.A., Stervbo, U., Hilgenberg, E., Ries, S., Dang, V.D., Jaimes, Y., Daridon, C., et al. (2014). IL-35-producing B cells are critical regulators of immunity during autoimmune and infectious diseases. Nature *507*, 366–370.

Teichmann, L.L., Kashgarian, M., Weaver, C.T., Roers, A., Müller, W., and Shlomchik, M.J. (2012). B cell-derived IL-10 does not regulate spontaneous systemic autoimmunity in MRL.Fas(lpr) mice. J. Immunol. *188*, 678–685.

Thomas-Chollier, M., Hufton, A., Heinig, M., O'Keeffe, S., Masri, N.E., Roider, H.G., Manke, T., and Vingron, M. (2011). Transcription factor binding predictions using TRAP for the analysis of ChIP-seq data and regulatory SNPs. Nat. Protoc. *6*, 1860–1869.

Tiller, T., Busse, C.E., and Wardemann, H. (2009). Cloning and expression of murine Ig genes from single B cells. J. Immunol. Methods *350*, 183–193.

Wang, Z.Y., Sato, H., Kusam, S., Sehra, S., Toney, L.M., and Dent, A.L. (2005). Regulation of IL-10 gene expression in Th2 cells by Jun proteins. J. Immunol. *174*, 2098–2105.

Workman, C.J., Cauley, L.S., Kim, I.J., Blackman, M.A., Woodland, D.L., and Vignali, D.A. (2004). Lymphocyte activation gene-3 (CD223) regulates the size of the expanding T cell population following antigen activation in vivo. J. Immunol. *172*, 5450–5455.

Wu, Z., Irizarry, R.A., Gentleman, R., Martinez-Murillo, F., and Spencer, F. (2004). A model-based background adjustment for oligonucleotide expression arrays. J. Am. Stat. Assoc. *99*, 909–917.

Yanaba, K., Bouaziz, J.D., Haas, K.M., Poe, J.C., Fujimoto, M., and Tedder, T.F. (2008). A regulatory B cell subset with a unique CD1dhiCD5+ phenotype controls T cell-dependent inflammatory responses. Immunity *28*, 639–650.

Yang, M., Deng, J., Liu, Y., Ko, K.H., Wang, X., Jiao, Z., Wang, S., Hua, Z., Sun, L., Srivastava, G., et al. (2012). IL-10-producing regulatory B10 cells ameliorate collagen-induced arthritis via suppressing Th17 cell generation. Am. J. Pathol. *180*, 2375–2385.

Yoshida, R., Suzuki, M., Sakaguchi, R., Hasegawa, E., Kimura, A., Shichita, T., Sekiya, T., Shiraishi, H., Shimoda, K., and Yoshimura, A. (2012). Forced expression of stabilized c-Fos in dendritic cells reduces cytokine production and immune responses in vivo. Biochem. Biophys. Res. Commun. *423*, 247–252.

STAR★METHODS

KEY RESOURCES TABLE

REAGENT or RESOURCE	SOURCE	IDENTIFIER
Antibodies		
B220	BioLegend	Clone RA3-6B2; RRID: AB_2563491
CD1d	BD PharMingen/BioLegend	Clone 1B1; RRID: AB_2073521, AB_1236543
CD3	BioLegend	Clone 145-2C11; RRID: AB_893317
CD4	BioLegend	Clone GK1.5 or RM4-5; RRID: AB_893323, AB_10898318
CD5	BD PharMingen/BioLegend	Clone 53-7.3; RRID: AB_394559, AB_2563930
CD8	BioLegend	Clone 53-6.7; RRID: AB_893423, AB_2561389
CD11b	BioLegend	Clone M1/70; RRID: AB_755986, AB_830642
CD11c	BioLegend	Clone N418; RRID: AB_830649, AB_389306
CD19	BioLegend	Clone 6D5; RRID: AB_493734, AB_830707
CD21/35	BD PharMingen/BioLegend	Clone 7G6/7E9; RRID: AB_395070, AB_1953277
CD23	BD PharMingen/BioLegend	Clone B3B4; RRID: AB_394652, AB_2103038, AB_312829
CD24	BioLegend	Clone M1/69; RRID: AB_2563464
CD40L	Miltenyi Biotec	Clone MR1; RRID: AB_2661127
CD40	DRFZ	Clone FGK-45
CD43	BD PharMingen	Clone S7; RRID: AB_10895376
CD69	DRFZ	Clone H1.2F3
CD71	BioLegend	Clone RI7217; RRID: AB_313564
CD72	BD PharMingen	Clone K10.6; RRID: AB_393982
CD79α	BioLegend	Clone F11-172; RRID: AB_2075634
CD79β	BioLegend	Clone HM79-12; RRID: AB_1575061
CD81	BioLegend	Clone Eat-2; RRID: AB_313138
CD93	eBioscience	Clone AA4.1; RRID: AB_469466
CD138	BD PharMingen/BioLegend	Clone 281-2; RRID: AB_395000, AB_2565621
CD200	BioLegend	Clone OX-90; RRID: AB_10900996
CXCR3	BioLegend	Clone CXCR3-173; RRID: AB_1088994
Foxp3	eBioscience	Clone FJK-16 s; RRID: AB_465243, AB_465936
Fc receptor	DRFZ	Clone 2.4G2
FAS	BD PharMingen	Clone Jo2; RRID: AB_396768
GL-7	BD PharMingen	Clone GL7; RRID: AB_10894953
IgM	BioLegend	Clone RMM-1; RRID: AB_2650758
IgD	BioLegend	Clone 11-26c.2a; RRID: AB_2562887
IFN-γ	BD PharMingen/BioLegend	Clone XMG1.2; RRID: AB_2034014, AB_1595591
Ki-67	BioLegend	Clone 16A8; RRID: AB_2561929
LAG-3 (CD223)	eBioscience	Clone C9B7W; RRID: AB_494214, AB_2573428
MHC-II	DRFZ	Clone M5/114
PD-1	BioLegend	Clone 29F.1A12; RRID: AB_2251944
TCR-β	BD PharMingen	Clone H57-597; RRID: AB_10584335
TNF-α	BD PharMingen/BioLegend	Clone MP6-XT22; RRID: AB_2562918, AB_469508
PD-L1	BD PharMingen	Clone MIH5; RRID: AB_397018
PD-L2	BioLegend	Clone TY25; RRID: AB_2566345
VH11	Prof. Kyoko Hayakawa (Fox Chase Cancer Center, Philadelphia, USA)	Clone P18-3H7

(*Continued on next page*)

Continued

REAGENT or RESOURCE	SOURCE	IDENTIFIER
Vk14 (Vk9)	Prof. Kyoko Hayakawa (Fox Chase Cancer Center, Philadelphia, USA)	Clone P18-13B5
VH12	Prof. Klaus Rajewsky (MDC Berlin)	Clone 5C5
IL-10	BioXCell	Clone JES5-2A5; RRID: AB_1107696
IL-10R	BioXCell	Clone 1B1.3A; RRID: AB_1107611
Ig (H+L)	Southern Biotechnology	Cat. #1010-01; RRID: AB_609680
IgM-AP	Southern Biotechnology	Cat. #1020-04; RRID: AB_619829
IgG-AP	Southern Biotechnology	Cat. #1030-04; RRID: AB_609689
IgG1-AP	Southern Biotechnology	Cat. #1070-04
IgG2b-AP	Southern Biotechnology	Cat. #1090-04; RRID: AB_619828
IgG2c-AP	Southern Biotechnology	Cat. #1079-04; RRID: AB_2692321
IgG3-AP	Southern Biotechnology	Cat. #1100-04
IgA-AP	Southern Biotechnology	Cat. #1040-04; RRID: AB_619826
Goat Anti-Human IgG-UNLB	Southern Biotech	Cat. #2040-01; RRID: AB_617099
Goat Anti-Human IgG-Biotin	Southern Biotech	Cat. #2040-08
Human IgG standard	Sigma-Aldrich	Cat. #I2511; RRID: AB_1163604
Streptavidin-Alexa 488	Thermo Fisher Scientific	Cat. #S32354
Streptavidin-PE	BD PharMingen	Cat. #554061
Streptavidin-APC	BD PharMingen	Cat. #554067
Streptavidin-APC-Cy7	BioLegend	Cat. #405208
Streptavidin-BV421	BioLegend	Cat. #405225
Streptavidin-BV605	BioLegend	Cat. #405229
Streptavidin-BV785	BioLegend	Cat. #405249
Streptavidin-PE/Cy7	BD PharMingen	Cat. #557598
Streptavidin-PerCP	BD PharMingen	Cat. #554064
Anti-PE	Miltenyi Biotec	Cat. #130-048-801; RRID: AB_244373
B-1a Cell Isolation Kit	Miltenyi Biotec	Cat. #130-097-413
CD19	Miltenyi Biotec	Cat. #130-052-201
CD43	Miltenyi Biotec	Cat. #130-049-801
CD11b	Miltenyi Biotec	Cat. #130-049-601
CD11c	Miltenyi Biotec	Cat. #130-052-001
CD4	Miltenyi Biotec	Cat. #130-049-201
CD8	Miltenyi Biotec	Cat. #130-049-401
CD90.2	Miltenyi Biotec	Cat. #130-049-101
Chemical Peptides and Recombinant Proteins		
DAPI	Sigma	Cat. #D8417
Propidium Iodide	Sigma	Cat. #P4864
Glutaraldehyde	Electron Microscopy Sciences	Cat. #16220
Osmiumtetroxide	Polysciences	Cat. #0223D
Tannic acid	Polysciences	Cat. #04459
Uranyl acetate	Ted Pella inc	Cat. #19481
CutSmart Buffer	NEB	Cat. #B7204S
Trypsin 0.5% EDTA	Life Technologies	Cat. #25300054
2-Mercaptoethanol	Life Technologies	Cat. #31350010
Calcium chlorure dihydrated	Roth	Cat. #5239.2
TMB	Ebioscience	Cat. #00-4201-56
Tween20	Sigma-Aldrich	Cat. #P1379

(*Continued on next page*)

Continued

REAGENT or RESOURCE	SOURCE	IDENTIFIER
Critical Commercial Assays		
Gene Chip Mouse 430 2.0	Affymetrix GmbH	Cat. #900495
Mouse Cell Screening (PE) kit	BioLegend	Cat. #700003
Foxp3 Staining Buffer Set	Ebioscience	Cat. #00-5523-00
BD Cytofix/Cytoperm Plus Kit	BD PharMingen	Cat. #554715
One Step RT-PCR kit	QIAGEN	Cat. #210212
Reverse Transcription System	Promega	Cat. #A3500
LightCycler FastStart DNA MasterPLUS SYBR Green	Roche Diagnostik	Cat. #03515885001
Bio-Plex Pro Mouse Cytokine IL-10 Set, 1 × 96 well	Bio-Rad	Cat. #171-G5009M
Deposited Data		
Gene array data	This paper	GEO: GSE103458
RNA-seq and DNA methylation data	This paper	ENA: PRJEB22138
Other		
Expression vectors containing the human IGG1 constant regions	Prof. Dr. Hedda Wardemann, (DKFZ, Heidelberg)	N/A
Expression vectors containing the human IGK constant regions	Prof. Dr. Hedda Wardemann, (DKFZ, Heidelberg)	N/A
Expression vectors codings for Human monoclonal antibody mGO53	Prof. Dr. Hedda Wardemann, (DKFZ, Heidelberg)	N/A
Expression vectors codings for Human monoclonal antibody JB40	Prof. Dr. Hedda Wardemann, (DKFZ, Heidelberg)	N/A
Expression vectors codings for Human monoclonal antibody ED38	Prof. Dr. Hedda Wardemann, (DKFZ, Heidelberg)	N/A
PtC-containing Liposomes labeled with Texas Red	FormuMax	Cat. #F60103F-TR
Lipopolysaccharides from *Escherichia coli* 055:B5	Sigma	Cat. #L2637-25MG
Tamoxifen	Sigma	Cat. #T5648-1G
Sunflower seed oil from Helianthus annuus	Sigma	Cat. #S5007-250ML
NP-KLH	BioCat GmbH	Cat. # N-5060-25
NP-LPS	BioCat GmbH	Cat. # N-5065
NP-AECM-FICOLL	BioCat GmbH	Cat. # F-1420
AffiniPure Fab2 Fragment Goat Anti-Mouse IgM	Dianova GmbH	Cat. #115-006-075
MacConkey Agar	Becton Dickinson GmbH	Cat. #212123
RNeasy Mini Kit	QIAGEN	Cat. #74106
Recombinant murine IL-6 protein	R&D Systems GmbH	Cat. #406-ML-005
Recombinant murine IL-21 protein	R&D Systems GmbH	Cat. #594-ML-010
MultiScreenHTS IP Filter Plate	Millipore	Cat. #MSIPN4510
BCIP/NBT substrate	Thermo Fisher Scientific	Cat. #34042
Proteinase K	Sigma Aldrich	Cat. #P2308
Pefabloc SC	Sigma Aldrich	Cat. #76307
HaeIII	New England Biolabs	Cat. #R0108M
Klenow Fragment exo-	New England Biolabs	Cat. #M0212L
T4-Ligase	New England Biolabs	Cat. #M0202M

(*Continued on next page*)

Continued

REAGENT or RESOURCE	SOURCE	IDENTIFIER
T4-Ligase	New England Biolabs	Cat. #M0202L
RNase H	New England Biolabs	Cat. #M0297L
DNA Polymerase I	New England Biolabs	Cat. #M0209L
NEBNext High-Fidelity 2X PCR Master Mix	New England Biolabs	Cat. #M0541L
TruSeq DNA PCR-Free LT Library Preparation Kit - Set A	Illumina	Cat. #FC-121-3001
Nextera DNA Sample Preparation Kit	Illumina	Cat. #FC-121-1030
EZ DNA Methylation-Gold Kit	Zymo research	Cat. #D5006
HotStarTaq DNA Polymerase	QIAGEN	Cat. #203207
MinElute PCR Purification Kit	QIAGEN	Cat. #28006
Agencourt AMPure XP	Beckman Coulter	Cat. #A63881
mRNA Capture Kit	Roche	Cat. #11787896001
M-MLV Reverse Transcriptase, RNase H Minus, Point Mutant	Promega	Cat. #M3683
Agilent High Sensitivity DNA Kit	Agilent	Cat. #5067-4626
Pfu polymerase	Promega	Cat. #M7745
Hot Taq polymerase	Promega	Cat. #M7805
dNTP Master Mix	Eurogentec	Cat. #NU-0010-100
AgeI–HF	NEB	Cat. #R3552L
SalI–HF	NEB	Cat. #R3138L
BsiWI	NEB	Cat. #R0553L
NEBuffer 1	NEB	Cat. #B7001S
Gel and PCR clean up kit	Macherey-Nagel	Cat. #740609.250
10X Buffer T4 ligase	Promega	Cat. #C126A
T4 ligase	Promega	Cat. #M180B
One Shot TOP10 Chemically Competent E.coli	Invitrogen	Cat. #C404006
Luria Broth	Dutscher	Cat. #777495
Luria Agar	Dutscher	Cat. #777494
S.O.C Medium	Life Technologies	Cat. #15544034
Ampicillin sodium salt	Sigma-Aldrich	Cat. #A9518
NucleoSpin Plasmid	Macherey-Nagel	Cat. #740588.250
NucleoSpin 96 Plasmid Transfection-grade	Macherey-Nagel	Cat. #740491.4
DMEM	Life Technologies	Cat. #61965026
FBS South America	BIOWEST	Cat. #S1810-500
Penicillin/Streptomycin sol	Life Technologies	Cat. #15140-122
Nutridoma-SP	Sigma-Aldrich	Cat. #11011375001
Double strand DNA	Sigma-Aldrich	Cat. #31149-10G-F
Insulin	Sigma-Aldrich	Cat. #I9278-5ML
Bovine Serum Albumin	Sigma-Aldrich	Cat. #A7906-100G
Extravidin, Peroxidase Conjugate	Sigma-Aldrich	Cat. #E2886-1ML

CONTACT FOR REAGENT AND RESOURCE SHARING

Further information and requests for resources and reagents should be directed to and will be fulfilled by the Lead Contact, Simon Fillatreau (simonfillatreau@googlemail.com). Certain materials are shared with academic and non-profit research organizations for research and educational purposes only under an MTA to be discussed in good faith with the recipient.

EXPERIMENTAL MODEL AND SUBJECT DETAILS

Mice

C57BL/6, *Il10*eGFP (Neves et al., 2010), *Btk*$^{-/-}$, *Cd72*$^{-/-}$, *Cd19*$^{-/-}$, *Cd1d*$^{-/-}$, *Nos2*$^{-/-}$, *Rag2*$^{-/-}$, B1-8i*Igk*$^{-/-}$, *Fc*γ*r2b*$^{-/-}$, *Cd19*-cre-*Notch2*$^{fl/fl}$, *Il10*$^{-/-}$, *Lag3*$^{-/-}$ (Miyazaki et al., 1996, Workman et al., 2004), *Tcr*$\alpha/\beta^{-/-}$, *Cd40*$^{-/-}$, *Myd88*$^{-/-}$, *Myd88*$^{-/-}$*Trif*$^{-/-}$, J_HT, *Cd72*$^{-/-}$$J_HT$, *Prdm1*eGFP, *Cd72*$^{-/-}$*Il10*eGFP, *Lag3*$^{-/-}$*Il10*eGFP, *Cd21*-cre-ROSA-STOP-eYFP, *Aicda*-cre-ERT2-ROSA-STOP-RFP, C3H/HeOuJ were bred under specific pathogen-free conditions. C3H/HeOuJ mice were also bred under germ-free conditions. Mouse strains used in infection experiments were NrampS. B-*Lag3*$^{-/-}$ mice were obtained by reconstituting recipient mice with a mixture of bone marrow cells from B cell-deficient J_HT mice (80%) and *Lag3*$^{-/-}$ mice (20%). Control B-WT chimera was obtained using a mixture of bone marrow cells from J_HT mice (80%) and C57BL/6 mice (20%). B-*Lag3*$^{-/-}$*Il10*eGFP and their B-*Il10*eGFP controls were obtained using the same strategy. All experiments were reviewed and approved by appropriate institutional review committees (LAGeSo Berlin), and were conducted according to French, and German legislations, in compliance with European community council directive 68/609/EEC guidelines. Mice were of C57BL/6 strain, 6-14 weeks old at start of experiments, unless otherwise stated, and of sex-matched male and female genders.

METHOD DETAILS

Bacterial infection

Mice were infected with $1x10^6$ or $1x10^7$ CFU for *Salmonella typhimurium* SL7207 strain or 100 CFU for SL1344 strain intravenously (i.v.). For survival and vaccination plus rechallenge experiments mice were first vaccinated with $1x10^6$ CFU of SL7207 given i.v. and 90 days later were rechallenged with 100 CFU of SL1344 or $1x10^6$ or 10^7 CFU of SL7207. During survival experiments, mice were daily checked and presented as percentage of live animals. The bacterial loads were determined by plating a series of dilutions of homogenized organs on MacConkey agar plates. Heat-killed *S. typhimurium* (HKST) was prepared by inactivation of the SL1344 strain in water bath at 70°C for 1 hour. Bacteria were suspended in PBS. *Salmonella* infection was performed in a blinded manner, and identities of the mice were revealed upon termination of the experiment. No randomization was used. Estimation of size groups was based on our previous experience with these disease models, without *a priori* determination via power calculation. For neutralization of IL-10 signaling, mice were treated i.v. with a combination of anti-IL-10 (JES5-2A5; 500 μg/mouse/injection; BioXCell) and anti-IL-10R (1B1.3A; 500 μg/mouse/injection; BioXCell) on days −3, −1, and +1 after infection.

Tamoxifen administration

Tamoxifen was resuspended in sunflower seed oil from Helianthus annuus to a final concentration of 20mg/ml. 10mg of tamoxifen was administered by gavage to *Aicda*-cre-ERT2-ROSA-STOP-RFP mice twice with 5 days interval between the first and second administration. Mice were analyzed 15 days after the last administration.

Immunization and treatment with agonists of BCR, CD40, TLR4

C57BL/6 mice were immunized i.p. with 200 μg NP-KLH precipitated in alum, NP-Ficoll, or NP-LPS. Mice were analyzed 7 days after immunization. In house conjugated APC or PE nitrophenyl hapten was used to detected NP specific B and plasmocytes.

*Il10*eGFP mice were injected i.v. with 100 μg anti-BCR (Fab2 anti-mouse IgM), 50 μg anti-CD40 (FGK-45), or 10 μg LPS (*E. coli* 055:B5), alone or in combination. Mice were analyzed 24h later.

Isolation of plasmocytes and B cells

For gene array, quantitative PCR, restimulation *in vitro*, ELISPOT assays and transmission electron microscopy analysis, plasmocytes and B cell subsets were obtained from C57BL/6 or *Il10*eGFP mice, naive or on day 1 p.i. with 10^7 CFU *Salmonella* (SL7207) by a two steps process. First, CD138$^+$ cells were enriched by autoMACS after incubation with anti-CD138-PE followed by anti-PE microbeads. CD138$^+$ cells obtained after autoMACS were then stained with anti-CD19, CD138, LAG-3, CD22 and CD11b/CD11c/TCR-β/DAPI. The following populations were sorted by FACS Sorter Aria I and/or II from this fraction: CD138^{hi}CD22$^+$LAG-3$^-$CD11b$^-$CD11c$^-$TCR$^-$β$^-$DAPI$^-$, CD138^{hi}CD22$^-$LAG-3$^-$CD11b$^-$CD11c$^-$TCR$^-$β$^-$DAPI$^-$, CD138^{hi}CD22$^-$LAG-3$^+$CD11b$^-$CD11c$^-$TCR$^-$β$^-$DAPI$^-$, CD138^{hi}CD11b$^-$CD11c$^-$TCR$^-$β$^-$DAPI$^-$, CD138^{hi}*Il10*eGFP$^+$CD11b$^-$CD11c$^-$TCR-β$^-$DAPI$^-$ and CD138^{hi}*Il10*eGFP$^-$CD11b$^-$CD11c$^-$TCR-β$^-$DAPI$^-$, CD138^{hi}LAG-3$^+$CD11b$^-$CD11c$^-$TCR-β$^-$DAPI$^-$ and CD138^{hi}LAG-3$^-$CD11b$^-$CD11c$^-$TCR-β$^-$DAPI$^-$. The cells from the CD138-negative fraction after autoMACS were stained with anti-CD19, CD138, CD1d, CD21, CD23 and CD11b/CD11c/TCR-β/DAPI. CD19$^+$CD138$^-$CD11b$^-$CD11c$^-$TCRβ$^-$DAPI$^-$; CD19$^+$CD1d^{hi}CD11b$^-$CD11c$^-$TCR-β$^-$DAPI$^-$ and CD19$^+$CD1d^{low}CD11b$^-$CD11c$^-$TCR-β$^-$DAPI$^-$; CD19$^+$CD1d^{low}CD21$^+$CD23$^+$CD11b$^-$CD11c$^-$TCR$^-$β$^-$DAPI$^-$ (FO) and CD19$^+$CD1d^{high}CD21^{high}CD23$^{low/-}$CD11b$^-$CD11c$^-$TCR$^-$β$^-$DAPI$^-$ (MZ) were then isolated from this fraction by FACS Sorter Aria I and/or II. Total B cells were obtained by magnetic isolation using negative selection with anti-CD11b, CD11c, and CD43 microbeads. For PeC, cells were incubated with B-1a Cell Biotin-Antibody Cocktail (Miltenyli Biotec) for 5 minutes at 2-8°C and then with anti-Biotin Microbeads for an additional 10 minutes in the same conditions in order to deplete non-B cells, according to Manufacturer's instructions. LD columns were used for removing the non-B cells. Unlabeled cells were collected representing the pre-enriched B1a cell fraction that contained all PeC B cells fractions.

For single cell sorting, single CD138^{hi}*Il10*eGFP^{+}CD11b^{-}CD11c^{-}TCR-β^{-}DAPI^{-} or CD138^{hi}*Il10*eGFP^{-}CD11b^{-}CD11c^{-}TCR-β^{-}DAPI^{-}, CD138^{hi}LAG-3^{+}CD11b^{-}CD11c^{-}TCR-β^{-}DAPI^{-}, CD138^{hi}LAG-3^{-}CD11b^{-}CD11c^{-}TCR-β^{-}DAPI^{-} plasmocytes were directly sorted into 96-well PCR plates supplemented 1X RT-PCR buffer. Plates were then covered with microseal B film and immediately frozen on dry ice before storage at −80°C for further experiments.

For epigenetic and RNaseq analysis plasmocyte and B cell populations were sorted by FACS Sorter Aria I and/or II from spleen and PeC of naive C57BL/6 mice using the gating strategy illustrated in Methods S1.

For adoptive transfer, 10^6 of flow cytometry-sorted B1a, B1b, and B2 cells from PeC, as well as CD19^{+}CD138^{-} splenic B cells were administered i.p. into *Rag2*$^{-/-}$ mice, which were analyzed 3 weeks later.

B cell stimulation and cytokine production measurement

Plasmocytes and/or B cell subsets were stimulated at 5x10^5 or 1x10^5 cells per well in 96-well flat or round bottom plates, respectively, in complete RPMI or with LPS (1μg/ml), α-IgM (Fab) (Dianova GmbH, 5μg/ml), agonistic α-CD40 antibody (clone FGK-45, produced in house at 10μg/ml), and in combinations in the presence of IL-6 (20ng/ml; R&D Systems GmbH), IL-21 (20ng/ml; R&D Systems GmbH). For analysis of cytokine production, 150μl supernatant of activated cells was collected and transferred into new 96 well plates and kept at −20°C until further use. 50μl of supernatant was used to measure cytokine concentration using Bio-Plex kits (Bio-Rad) according to the manufacturer's instruction.

Transmission Electron Microscopy

Sorted cells, fixed in 2.5% glutaraldehyde (EM grade), were sedimented in warm low melting agarose (2% in PBS) and left to set. Excised bits of agarose containing cell-groups were then postfixed in 0.5% osmium tetroxide, contrasted with tannic acid and 2% uranyl acetate, dehydrated in a graded ethanol series and embedded in epoxy resin. After polymerization, sections were cut at 60 nm and contrasted with lead citrate. Specimens were analyzed in a Leo 906E transmission electron microscope at 100KV (Zeiss, Oberkochen, DE) using a side mounted digital camera (Morada; SIS-Olympus Münster DE).

Gene array hybridization

cRNA were hybridized on Affymetrix MG 430 2.0 arrays using standard Affymetrix protocol after quality control with Agilent 2100 Bioanalyzer and quantification with NanoDrop ND-1000 spectrophotometer.

Library preparation for methylation analysis of plasmocytes and B cell subsets

Sorted cells were lysed and digested with proteinase K followed by addition of 1mM Pefabloc SC (Sigma-Aldrich) to inhibit protease activity. Cell lysates were digested overnight with 50U HaeIII (New England Biolabs) followed by inactivation at 80°C. A-tailing was performed using 5U Klenow exo^{-} (New England Biolabs), and Illumina TruSeq adaptors were ligated at 16°C overnight using 2000U T4-Ligase (New England Biolabs). DNA fragments were purified with 1.5x Agencourt AMPure XP (Beckman Coulter) and bisulfite treated using the EZ DNA Methylation-Gold Kit (Zymo research) following the manufacturer's protocol. The libraries were amplified by 14-15 cycles of PCR using HotStarTaq DNA Polymerase (QIAGEN), and purified with 0.9x Agencourt AMPure XP (Beckman Coulter). The library quality was assessed using Agilent 2100 Bioanalyzer, and the quantity was measured using Qubit® dsDNA HS Assay Kit (Thermo Fisher Scientific). The Illumina HiSeq 2500 system was used for 100 bp single-end sequencing.

Library preparation for mRNA Seq

mRNA Capture Kit (Roche) was used to isolate mRNA with the modification that cell pellets (10^5 cells) were lysed in 49μl lysis buffer, and 1μl of the biotin labeled oligo(dT)$_{20}$ working solution was added to the lysate. After immobilization and washing of mRNA in streptavidin coated tubes first strand synthesis was performed in 50μl using 400U M-MLV Reverse Transcriptase RNase H^{-} (Promega) at 37°C for 1h. For second strand synthesis 400U T4-Ligase, 5U RNase H, and 50U DNA Polymerase I (New England Biolabs) were used at 16°C for 2.5h. The double stranded cDNA was fragmented and tagged with sequencing adapters using the Nextera DNA Library Preparation Kit (Illumina) with the deviation that 0.2μl of the Tagment DNA Enzyme 1 were used in a 50μl reaction. After incubation at 55°C for 5 minutes the reaction was stopped and the DNA was released from the tubes by the addition of 250μl of Buffer PB (QIAGEN). The DNA was purified using MinElute PCR Purification Kit (QIAGEN) following the manufacturer's protocol, and the elution step was performed with 11.5μl distilled water. The libraries were amplified for 12 cycles using NEBNext High-Fidelity 2X PCR Master Mix (New England Biolabs) and 0.2μM Index adapters (AATGATACGGCGACCACCGAGATCTACAC[i5]TCGTCGGCAGCGTC and CAAGCAGAAGACGGCATACGAGAT[i7]GTCTCGTGGGCTCGG). The libraries were purified with 0.8x Agencourt AMPure XP (Beckman Coulter), and sequenced using the Illumina HiSeq 2500 system with 1x100 bp single-end reads.

Analysis of mRNA expression by B cells and plasmocytes

Sorted or cultured B cells and plasmocytes were lysed in RLT buffer (QIAGEN) and kept at −80°C until use. Total RNA was extracted using RNeasy Mini Kit (QIAGEN) according to the manufacturer's instruction. After DNase treatment, cDNA was synthesized from RNA with a Reverse Transcription System (Promega). Quantitative RT-PCR was performed on an MX3005P QPCR System (Stratagene), with LightCycler FastStart DNA Master SYBR Green I (Roche). Transcripts were quantified using β-actin as standard, and the

following forward (FP) and reverse (RP) primers (MWG Biotech): β-actin FP: 5′-TGGAATCCTGTGGCATCCATGAAAC-3′, β-actin RP: 5′-TAAAACGCAGCTCAGTAACAGTCC-3′; IL-10 FP: 5′-AGCCGGGAAGACAATAAC TG-3′, IL-10 RP: 5′-CATTTCCGA TAAGGCTTG G-3′.

Ig gene amplification from single cells

Single cells sorted in 96-well PCR plate were immediately frozen on dry ice and stored at −80°C until further use. To amplify Ig gene from single cells, a nested PCR approach was used. Reverse transcription (RT) and the first PCR step for *Igμ* (IgM) and *Igκ* variable gene transcripts were carried out in a one-step reaction using the QIAGEN OneStep RT-PCR kit according to the manufacturer's instructions. The Ig gene primers were chosen based on Tiller et al. (2009). The second round of PCR was carried out with 2μl of a 100-fold dilution of the unpurified first PCR product at 94°C for 4 minutes followed by 50 cycles of 94°C for 30 s, 60°C (*Igμ*) or 48°C (*Igκ*) for 30 s, 72°C for 45 s, and final incubation at 72°C for 10 minutes. The second PCR products were analyzed on 2% agarose gels.

The Ig gene PCR products from different plasmocyte subsets were sequenced (LGC) with the respective forward primers. Nucleotide sequences were then analyzed using IMGT/V-Quest to determine germline V, D, and J gene members, somatic hypermutation (counted for CDR1-FWR3 inclusively), CDR3 sequences, N-nucleotide addition.

Cloning of mouse Ig genes into expression vectors

After identifying V and J gene segment, second PCR reactions were repeated using 5μl of a 100-fold dilution of the unpurified first PCR product as template with specific V and J gene primers containing restriction sites to clone directly into expression vectors. PCR products were purified using Gel and PCR clean up kit before digestion with AgeI and SalI (Igh), AgeI and BsiWI (Igk). Digested Igh and Igk PCR products were purified from 0.9% agarose before ligation into expression vectors containing the human IGG1 and IGK constant regions, respectively. Ligation products were transformed into competent *E.Coli* via heat shock at 42°C, then *E.Coli* cells were plated on Ampicillin plates (100μg/ml) overnight at 37°C. Inserted genes were screened by PCR in Ampicillin resistant bacterial colonies.

Expression of recombinant immunoglobulin

Four single positively bacterial clones of each Igh and Igk gene were grown overnight at 37°C in 5ml of LB medium containing 100μg/ml Ampicillin. Plasmids were purified using NucleoSpin Plasmid - plasmid Miniprep kit (Macherey-Nagel), followed with digestion and analysis on 1% agarose. Inserted plasmids were then sequenced (GATC) to confirm identity with the second round PCR product and no mutation which probably is introduced by polymerase.

One day before transfection, $4x10^6$ HEK293 T cells were plated in T175 culture flasks in complete DMEM (DMEM + 10% (v/v) FCS + Penicillin (100U/ml)/Streptomycin (100 μg/ml) + 2-Mercaptoethanol (50 μM). The cell should be 80% confluency on the day of transfection. Transient transfections were performed with calcium-phosphate precipitation. In brief, equal amounts of IgH (7μg) and corresponding IgK chain vector were mixed with sterile water and 124μl of 2M $CaCl_2$. An equal volume of 1ml of 2X HBS was added drop-wise to the above mixture under slow vortexing and incubated at room temperature for 15min to allow formation of precipitates. The resulting solution was distributed to the culture flask. On the next day, cells were washed with 5ml of serum-free DMEM and 20ml of DMEM supplemented with 1% Nutridoma-SP, Penicillin (100U/ml)/Streptomycin (100 μg/ml) and 2-Mercaptoethanol (50 μM) was added. Supernatant were harvested at day 6 post transfection, cell debris was removed by centrifugation at 800 g for 10 minutes and culture supernatants were stored at −20°C.

Detection of antibody reactivity by ELISAs

IgG concentration in the supernatants were determined by ELISA. In brief, enhanced protein-binding ELISA plates were coated with 50μl of Goat Anti-Human IgG-UNLB diluted in carbonate buffer as capture antibody at 4°C overnight. Plates were washed 3 times with PBS. Unspecific binding was blocked by 200μl PBS/ 3%BSA for 1 hour at 37°C and washed again 4 times with PBS/0.1% Tween. Human IgG standard and culture supernatants were added, incubated for 2 hours at 37°C and washed again to remove unbound antibody with PBS/0.1% Tween. 100μl of Biotinylated Goat Anti-Human IgG Secondary Antibody was added, incubated for 1 hour at room temperature and washed again with PBS/0.1% Tween prior to adding ExtrAvidin®−Peroxidase for 1 hour at room temperature. After washing, assays were developed using 100μl TMB solution and incubated at RT for color development. Assays were stopped by H_2SO_4 and ODs were measured at 450nm. Antibody concentration was determined by Softmax Pro software.

Antibodies with concentration higher than 5μg/ml were selected to test for polyreactivity with LPS, dsDNA and Insulin by ELISA. In brief, enhanced protein-binding ELISA plates were coated with 50μl of LPS (10μg/ml) or insulin (10μg/ml) or dsDNA (10μg/ml) in carbonate buffer and incubated at 4°C overnight. After washing, plates were incubated with 100μl nonpurified antibodies for 2 hours at 37°C and washed again. Nonpolyreactive (mGO53), low polyreactive (JB40), highly polyreactive (ED38) recombinant human monoclonal antibodies served as controls and were included on each plate. Unbound antibodies were removed by washing 4 times with PBS/0.1% Tween before detected using Biotinylated Goat Anti-Human IgG Secondary Antibody, followed with ExtrAvidin®−Peroxidase for 1 hour at room temperature. The rest steps were performed as above mentioned.

Cell staining for flow cytometry

For surface staining, splenocytes, BM, PeC, and lymph node cells were first incubated with anti-Fc receptor antibody (clone 2.4G2) for 15 minutes to block unspecific bindings, and surface staining was then performed with antibodies conjugated directly with fluorochrome for 15 minutes. For biotinylated antibodies, cells were further incubated with Streptavidin conjugated to fluorochrome for 15 minutes. Dead cells were excluded by DAPI or PI.

For cytokine intracellular staining, cells were plated at $5x10^6$ cells per well in flat-bottom 48-well plates with 1ml complete RPMI 1640 containing HKST for 1 hour. Golgistop was added afterward, and cells were incubated for 5 more hours. Cells were harvested and stained for surface markers, including uncoupled pacific orange to exclude dead cells before cells were fixed. Intracellular staining was performed with Cytofix/Cytoperm kit (BD) as recommended.

Ki67 (BioLegend) and Foxp3 nuclear stainings were performed with Foxp3 staining kit (Ebioscience). Stained cells were acquired on FACS Symphony, Fortessa, Canto, LSR II and analyzed with FlowJo software.

ELISPOT Assay

Sorted day 0 $CD138^{hi}$LAG-3^+ and $CD138^{hi}$LAG-3^- cells; day 1 $CD138^{hi}$*Il10*eGFP$^+$ and $CD138^{hi}$*Il10*eGFP$^-$ cells, and day 1 after re-challenge $CD138^{hi}$*Il10*eGFP$^+$ and $CD138^{hi}$ *Il10*eGFP$^-$ cells were seeded at a starting number of 10^4 cells per well, with seven successive three-folds serial dilutions, in MultiScreenHTS IP Filter Plate (Millipore) pre-coated with anti-mouse Ig(H+L) chain (5 μg/ml; Southern Biotechnology Associates, cat number 1010-01). After 3 h incubation, plates were washed, and incubated with alkaline phosphatase-conjugated anti-IgM or total IgG or IgG1 or IgG2b or IgG2c or IgG3 or IgA overnight at 4°C (Southern Biotechnology Associates). ELISPOT were then developed using BCIP/NBT substrate.

QUANTIFICATION AND STATISTIC ANALYSIS

Data and statistical analyses were performed using GraphPad Prism (GraphPad Software, USA) and data were represented as mean ± SEM. Equality of variances between groups was assessed before analyses by t test. Groups were compared using two-tailed t test, or Wilcoxon test, or Mann-Whitney test. t test was modified using Welch's correction in case of unequal variance ($^{ns}p > 0.05$, $^{*}p < 0.05$, $^{**}p < 0.01$; $^{***}p < 0.001$, $^{****}p < 0.0001$). No sample was excluded from analysis.

Gene array analysis

Normalization of microarrays was performed using gcrma R package (Wu et al., 2004). For each sample, we determined if a probe was present (i.e., expressed) or not using mas5calls function of affy R package (Gautier et al., 2004). The significantly differentially regulated genes were detected using limma R package (Ritchie et al., 2015) with p values adjusted according to Benjamini Hochberg procedure. In order to be selected in a comparison of two conditions, each Affy IDs had to fulfill the following criteria: (i) be present in at least two of the three arrays for at least one of the two conditions compared; (ii) to have a mean signal intensity higher than 50 in at least one of the two conditions; (iii) to show an adjusted (adj.) p value < 0.01 in the comparison of the two conditions. The genes differentially expressed between $CD138^{hi}$*Il10*eGFP$^+$ and $CD138^{hi}$*Il10*eGFP$^-$ plasmocytes (adj. p value < 0.01) were then selected and filtered using the gene ontology resource (www.geneontology.org) to focus on surface molecules. Heat-map of Figure 1A has been produced using pheatmap R package (pheatmap: Pretty Heatmaps. R package version 1.0.2. http://CRAN.R-project.org/package=pheatmap). If several probes were available for a given gene, their signal intensity has been averaged. For the hierarchical clustering, we used ward distance function and complete linkage function.

DNA methylation analysis

Trimming, alignment to the mm10 reference genome and DNA methylation value calling were performed as described before (Durek et al., 2016). Pairwise differential DNA methylation was calculated using the R package methylKit (Akalin et al., 2012) and DMR were defined as 1kb regions covering $\geq$ 3 CpG sites with $\geq$ 20% methylation difference (q-value $\leq$ 0.01) between the cell types. All analyzed CpG were filtered for coverage $\geq$ 10x and presence in all replicates. Average DNA methylation per cell type was calculated using coverage weighted average methylation of 3 replicates. DMR were annotated to genes and genomic location by using ChipSeek (Chen et al., 2014). Transcription factor binding sites were predicted using TRAP (Thomas-Chollier et al., 2011) and AliBaba2 (http://gene-regulation.com/pub/programs/alibaba2/index.html). The integrated Genome Viewer (IGV) genome browser was used to display data in Figure 4D and Figure S4D.

RNaseq analysis

Adaptor removal and trimming of low quality ends (phred score = 20) of FastQ format reads was performed using Trim Galore! (version 0.3.3) (http://www.bioinformatics.babraham.ac.uk/projects/trim_galore/). Alignment to the mm10 reference genome was done using 2-step STAR alignment (Dobin and Gingeras, 2015). PCR duplications were determined using MarkDuplicate (version 1.115) from Picard tools (http://broadinstitute.github.io/picard/) and quality control was performed using RNA-seQC (DeLuca et al., 2012). Subsequently, featureCounts (Liao et al., 2014) was used to count reads mapping to the genes from Gencode annotation (vM2) (https://www.encodeproject.org/files/gencode.vM2.annotation). Pairwise differential expression was analyzed using the R package edgeR (Robinson et al., 2010). A p value cutoff of 0.01 and an FDR cutoff of 0.05 was set to select differentially expressed genes. GO Term analysis were performed using GREAT (McLean et al., 2010).

DATA AND SOFTWARE AVAILABILITY

The Affymetrix gene array data have been deposited at NCBI GEO depository and are accessible with the accession number GSE103458, or using the link https://www.ncbi.nlm.nih.gov/geo/query/acc.cgi?acc=GSE103458

The RNaseq and DNA methylation data have been deposited at the European Nucleotide Archive (ENA), and will be accessible with the accession number PRJEB22138, or using the links.http://www.ebi.ac.uk/ena/data/view/PRJEB22138<https://deref-web-02.de/mail/client/dAlzMDs2lmY/dereferrer/?redirectUrl=http%3A%2F%2Fwww.ebi.ac.uk%2Fena%2Fdata%2Fview%2FPRJEB22138>

Immunity, Volume *49*

Supplemental Information

LAG-3 Inhibitory Receptor Expression Identifies Immunosuppressive Natural Regulatory Plasma Cells

Andreia C. Lino, Van Duc Dang, Vicky Lampropoulou, Anna Welle, Jara Joedicke, Jelka Pohar, Quentin Simon, Jessie Thalmensi, Aurelia Baures, Vinciane Flühler, Imme Sakwa, Ulrik Stervbo, Stefanie Ries, Luc Jouneau, Pierre Boudinot, Takeshi Tsubata, Takahiro Adachi, Andreas Hutloff, Thomas Dörner, Ursula Zimber-Strobl, Alex F. de Vos, Katja Dahlke, Gunnar Loh, Sarantis Korniotis, Christian Goosmann, Jean-Claude Weill, Claude-Agnès Reynaud, Stefan H.E. Kaufmann, Jörn Walter, and Simon Fillatreau

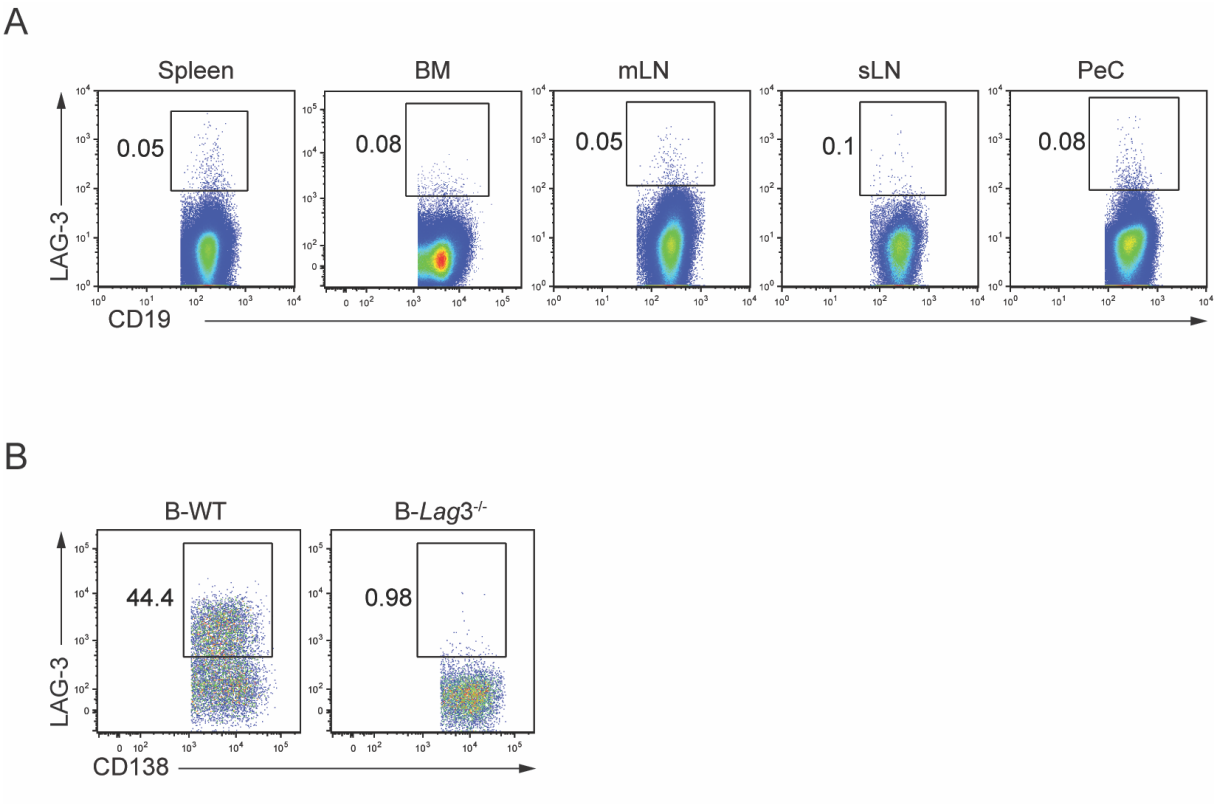

Figure S1: Expression of LAG-3 by B cells and plasmocytes in *Salmonella* infected mice, Related to Figure 1.

(A) Representative flow cytometry plots showing the expression of LAG-3 on $CD19^{+}CD138^{-}$ B cells from C57BL/6 mice in spleen, BM, mLN, sLN, and PeC on day 1 p.i. with *Salmonella* (SL7207, 10^7 CFU).

(B) Representative flow cytometry plots showing the expression of LAG-3 on splenic $CD138^{hi}$ cells of B-WT and B-*Lag3*$^{-/-}$ mice on day 1 p.i. with *Salmonella* (SL7207, 10^7 CFU).

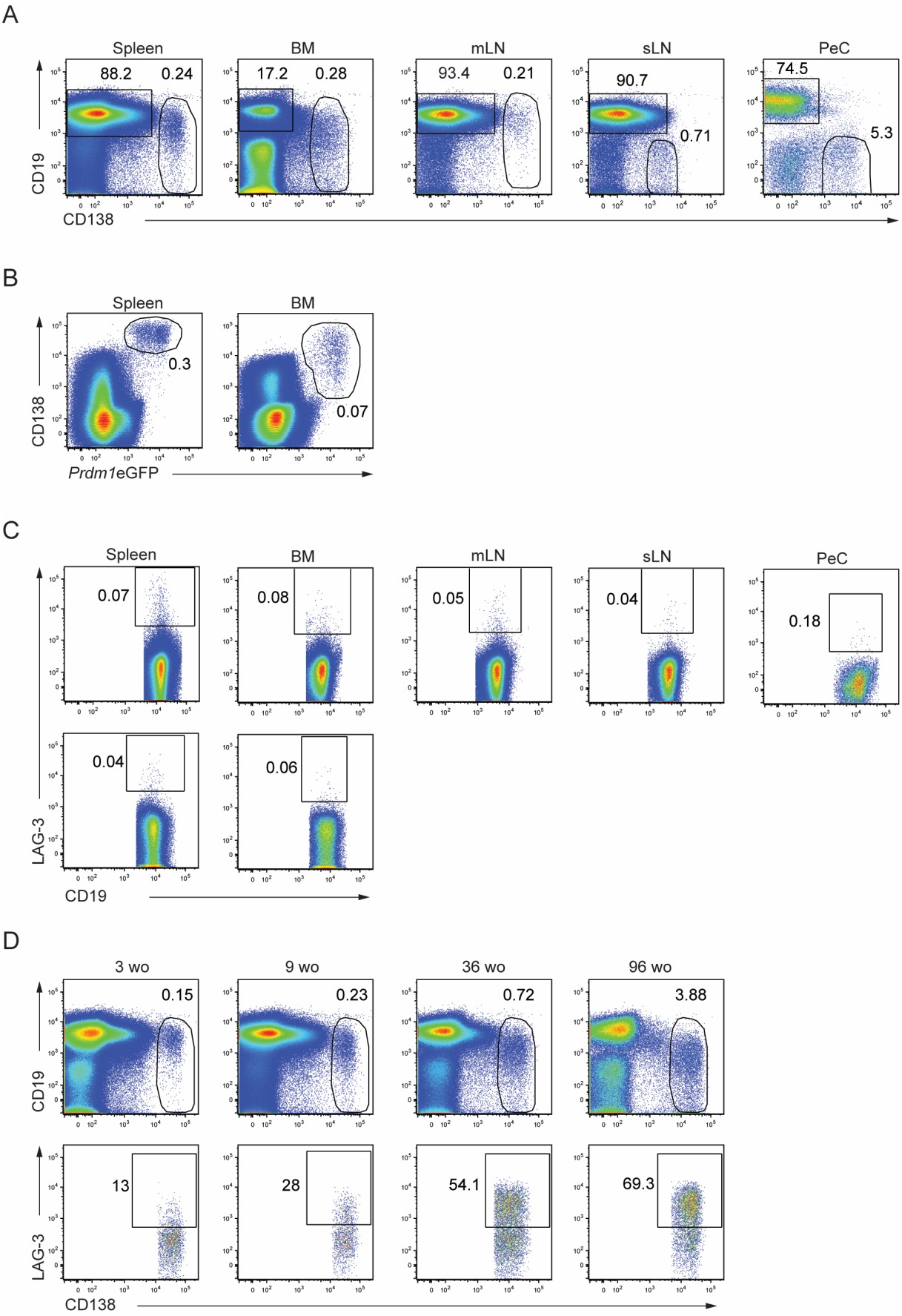
A
Spleen
BM
mLN
sLN
PeC
88.2
0.24
17.2
0.28
93.4
0.21
90.7
0.71
74.5
5.3
CD19
CD138
B
Spleen
BM
0.3
0.07
CD138
Prdm1eGFP
C
Spleen
BM
mLN
sLN
PeC
0.07
0.08
0.05
0.04
0.18
0.04
0.06
LAG-3
CD19
D
3 wo
9 wo
36 wo
96 wo
0.15
0.23
0.72
3.88
13
28
54.1
69.3
CD19
LAG-3
CD138

Figure S2: Presence of LAG-3-expressing plasma cells in naïve mice, Related to Figure 2.
(A) Representative flow cytometry plots showing the expression of CD19 and CD138 on live $CD4^-CD8^-$ lymphocytes in the indicated tissues. The gates identify $CD19^+CD138^-$ B cells characterized in Figure S2C, and $CD138^{+/hi}$ plasmocytes characterized in Figure 2A, for spleen, BM, mLN, sLN and PeC of naïve C57BL/6 mice.
(B) Representative flow cytometry plots showing the expression of CD138 and *Prdm1*eGFP on live $CD4^-CD8^-$ lymphocytes from spleen and BM of naïve *Prdm1*eGFP mice. The gates identify $CD138^{+/hi}$*Prdm1*$eGFP^+$ plasmocytes characterized in Figure 2B.
(C) Representative flow cytometry plots showing the expression of LAG-3 on $CD19^+CD138^-$ B cells in spleen, BM, mLN, sLN, and PeC from naïve C57BL/6 mice (top), as well as in spleen and BM from naïve *Lag3*$^{-/-}$ mice (bottom).
(D) Representative flow cytometry plots showing the expression of CD19 and CD138 in live $CD4^-CD8^-$ lymphocytes (top) and the expression of LAG-3 and CD138 in live $CD138^{hi}$ plasmocytes (bottom) from naïve C57BL/6 mice of indicated ages. The gates in top panels indicate $CD138^{hi}$ cells analysed for the expression of LAG-3 and CD138 in bottom panels.

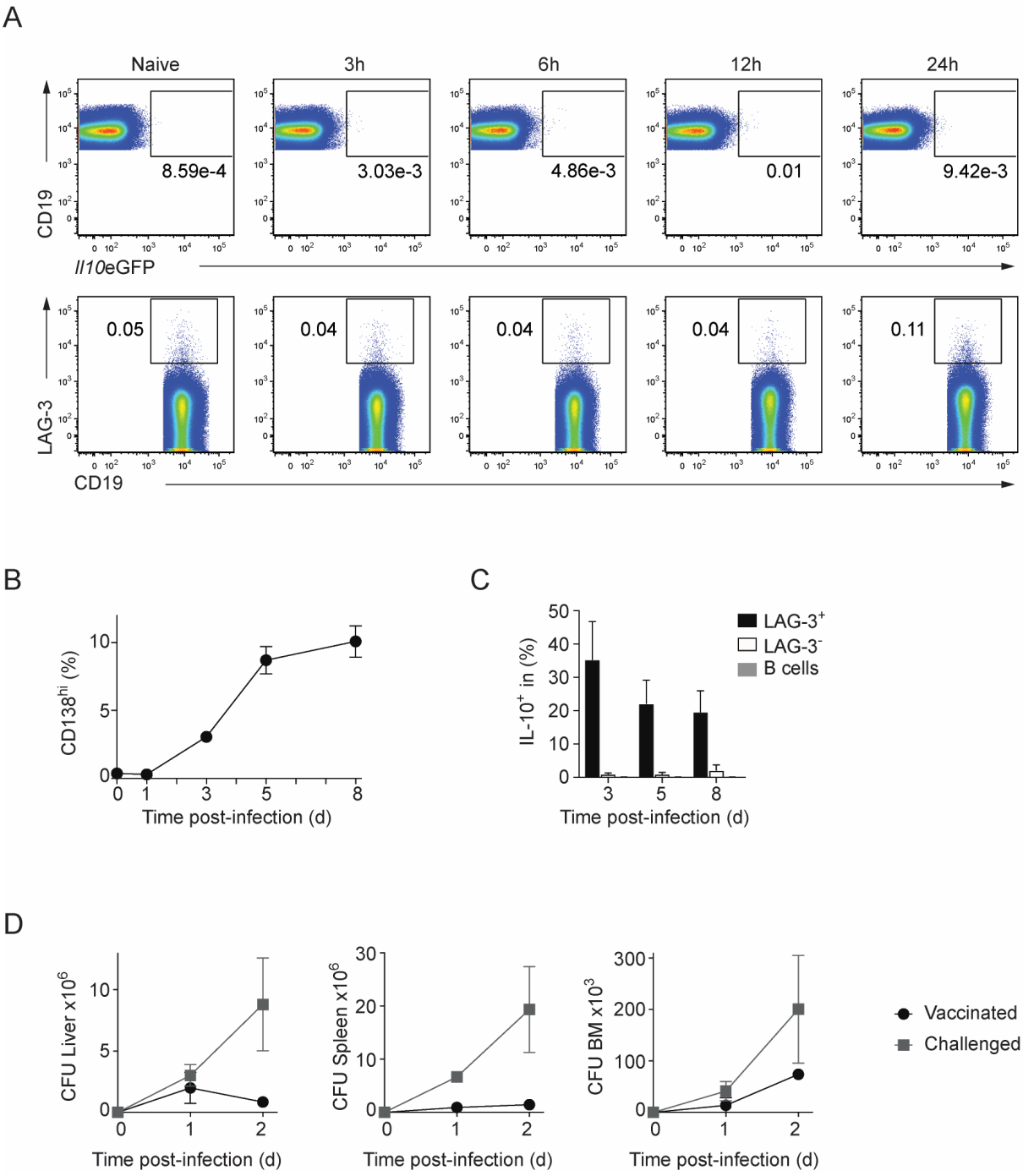
A
Naive
3h
6h
12h
24h
CD19
Il10eGFP
8.59e-4
3.03e-3
4.86e-3
0.01
9.42e-3
LAG-3
CD19
0.05
0.04
0.04
0.04
0.11
B
CD138hi (%)
Time post-infection (d)
C
IL-10+ in (%)
LAG-3+
LAG-3-
B cells
Time post-infection (d)
D
CFU Liver x10^6
CFU Spleen x10^6
CFU BM x10^3
Time post-infection (d)
Vaccinated
Challenged

Figure S3: Induction of IL-10 expression in LAG-3^{+}CD138^{hi} plasma cells during *Salmonella* infection, Related to Figure 3.

(A) *Il10*eGFP mice were challenged with *Salmonella* (SL7207, 10^7 CFU), and spleens were analysed at indicated hours p.i. Representative flow cytometry plots showing the expression of *Il10*eGFP and CD19 (top), and the expression of LAG-3 and CD19 (bottom) on live CD19^{+}CD138^{-} B cells.

(B) *Il10*eGFP mice were challenged with *Salmonella* (SL7207, 10^7 CFU). Data show the frequency of CD138^{hi} plasmocytes in CD4^{-}CD8^{-} live cells in spleen at indicated days p.i. Pool of two independent experiments with at least 6 mice per group.

(C) *Il10*eGFP mice were challenged with *Salmonella* (SL7207, 10^7 CFU), and spleens were analyzed at indicated days p.i. Data show frequencies of *Il10*eGFP^{+} cells in CD19^{+}CD138^{-} (B cells), LAG-3^{+}CD138^{hi} (LAG-3^{+}), and LAG-3^{-}CD138^{hi} (LAG-3^{-}) cells. Pool of two independent experiments with at least 6 mice per group

(D) *Il10*eGFP mice were vaccinated (SL7207, 10^6 CFU), and rechallenged 90 days later with *Salmonella* (SL7207, 10^7 CFU) together with naive age-matched control *Il10*eGFP mice. CFU were determined in liver (left), spleen (middle), and BM (right) at indicated days p.i. Data are pooled from two independent experiments with at least n=6 per group.

Data show mean ± SEM.

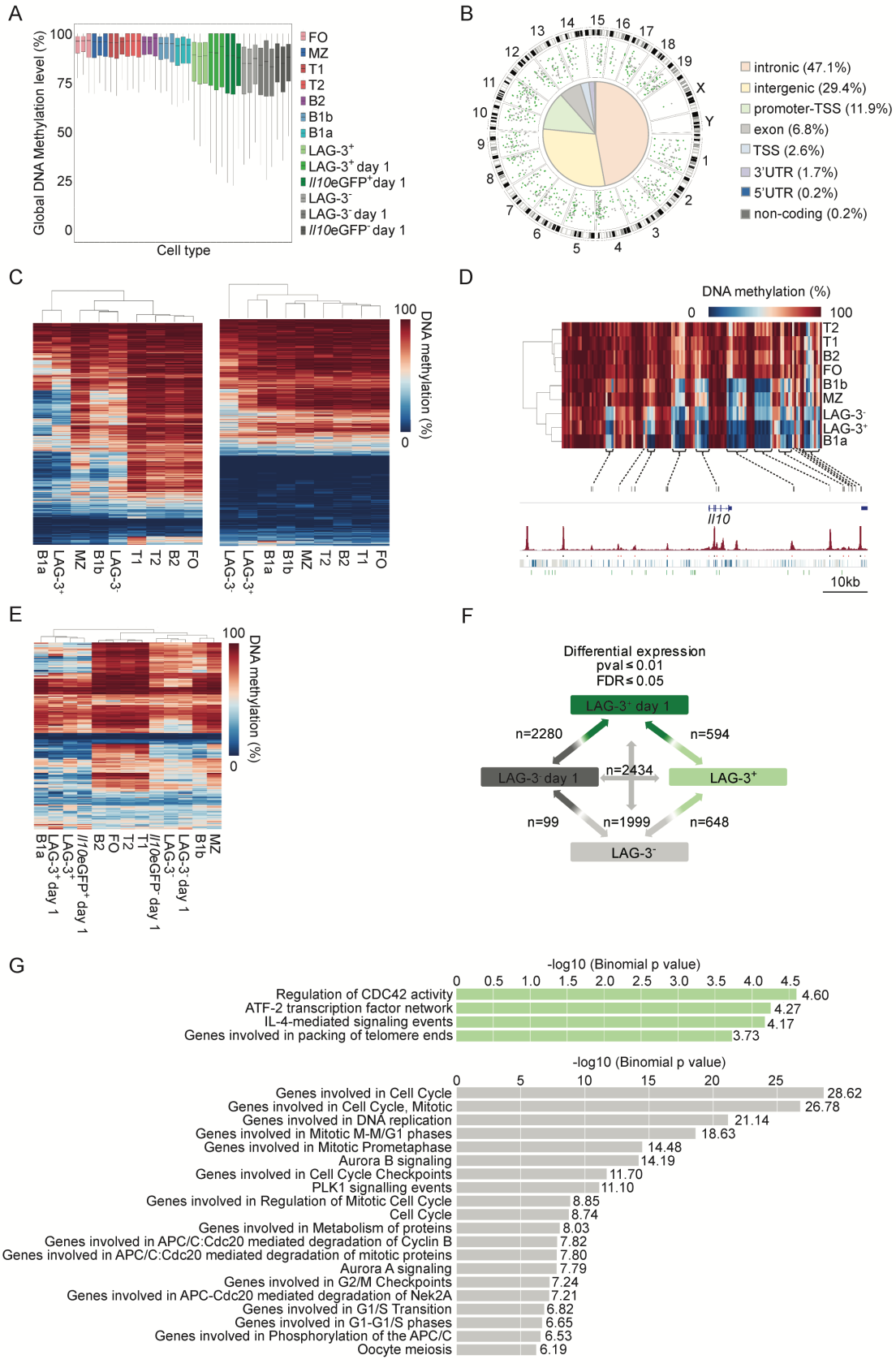
A
Global DNA Methylation level (%)
100
75
50
25
0
Cell type
FO
MZ
T1
T2
B2
B1b
B1a
LAG-3+
LAG-3+ day 1
Il10eGFP+day 1
LAG-3-
LAG-3- day 1
Il10eGFP- day 1
B
intronic (47.1%)
intergenic (29.4%)
promoter-TSS (11.9%)
exon (6.8%)
TSS (2.6%)
3'UTR (1.7%)
5'UTR (0.2%)
non-coding (0.2%)
C
DNA methylation (%)
100
0
B1a
LAG-3+
MZ
B1b
LAG-3-
T1
T2
B2
FO
D
DNA methylation (%)
0
100
T2
T1
B2
FO
B1b
MZ
LAG-3-
LAG-3+
B1a
Il10
10kb
E
DNA methylation (%)
100
0
B1a
LAG-3+ day 1
LAG-3+
Il10eGFP+ day 1
B2
FO
T2
T1
Il10eGFP- day 1
LAG-3-
LAG-3- day 1
B1b
MZ
F
Differential expression
pval ≤ 0.01
FDR ≤ 0.05
LAG-3+ day 1
n=2280
n=594
LAG-3- day 1
n=2434
LAG-3+
n=99
n=1999
n=648
LAG-3-
G
-log10 (Binomial p value)
0
0.5
1.0
1.5
2.0
2.5
3.0
3.5
4.0
4.5
Regulation of CDC42 activity 4.60
ATF-2 transcription factor network 4.27
IL-4-mediated signaling events 4.17
Genes involved in packing of telomere ends 3.73
-log10 (Binomial p value)
0
5
10
15
20
25
Genes involved in Cell Cycle 28.62
Genes involved in Cell Cycle, Mitotic 26.78
Genes involved in DNA replication 21.14
Genes involved in Mitotic M-M/G1 phases 18.63
Genes involved in Mitotic Prometaphase 14.48
Aurora B signaling 14.19
Genes involved in Cell Cycle Checkpoints 11.70
PLK1 signalling events 11.10
Genes involved in Regulation of Mitotic Cell Cycle 8.85
Cell Cycle 8.74
Genes involved in Metabolism of proteins 8.03
Genes involved in APC/C:Cdc20 mediated degradation of Cyclin B 7.82
Genes involved in APC/C:Cdc20 mediated degradation of mitotic proteins 7.80
Aurora A signaling 7.79
Genes involved in G2/M Checkpoints 7.24
Genes involved in APC-Cdc20 mediated degradation of Nek2A 7.21
Genes involved in G1/S Transition 6.82
Genes involved in G1-G1/S phases 6.65
Genes involved in Phosphorylation of the APC/C 6.53
Oocyte meiosis 6.19

Figure S4. Analysis of DNA methylation and gene expression, Related to Figure 4

(A) Boxplot showing the genome-wide methylation percentage for the indicated B lineage cell subsets.

(B) Circular representation showing the distribution of the 469 DMR identified between LAG-3^{+}CD138^{hi} cells and LAG-3^{-}CD138^{hi} cells from naïve mice across the chromosomes and the genome. The methylation frequency for each DMR is indicated for LAG-3^{+}CD138^{hi} cells (green dots) and LAG-3^{-}CD138^{hi} cells (grey dots). The genomic positions of the DMR on the chromosomes are given by their angular value, and their methylation ratio are indicated by their height from the centre (radius). The pie chart shows the global distribution of the DMR within functional genomic regions.

(C) Heat-maps displaying the methylation percentage of each CpG found in the 469 DMR (see Figure 4B) that are hypo-methylated (left) or hyper-methylated (right) in LAG-3^{+}CD138^{hi} cells compared to LAG-3^{-}CD138^{hi} cells.

(D) Heat-map showing the methylation ratio for all covered CpG positions in the *Il10* locus for the indicated B lineage cell subsets, and additional genomic information, as in Figure 4D. In addition, the location of Egr2 motifs is indicated by green bars.

(E) Heat-map displaying the methylation ratio for the DMR distinguishing LAG-3^{+}CD138^{hi} cells and LAG-3^{-}CD138^{hi} cells from naïve mice for the indicated B lineage cell subsets.

(F) Representation of the numbers of DEG (p-value $\leq$ 0.01 and FDR $\leq$ 0.05) for the indicated pairwise comparisons. The union of the ensembles of DEG contains 3631 elements.

(G) Gene set enrichment analysis for the DEG between LAG-3^{+}CD138^{hi} cells and LAG-3^{-}CD138^{hi} cells from naïve mice (MSigDB Pathway ontology). Upper and lower panels were obtained using the genes expressed at higher amounts in LAG-3^{+}CD138^{hi} cells, and LAG-3^{-}CD138^{hi} cells, respectively.

(B-E) Coverage weighted average methylation ratio from 3 replicates for each cell type are shown.

(A, E, F) All samples were from naïve mice except where indicated. (B, C, D, G) All samples were from naïve mice.

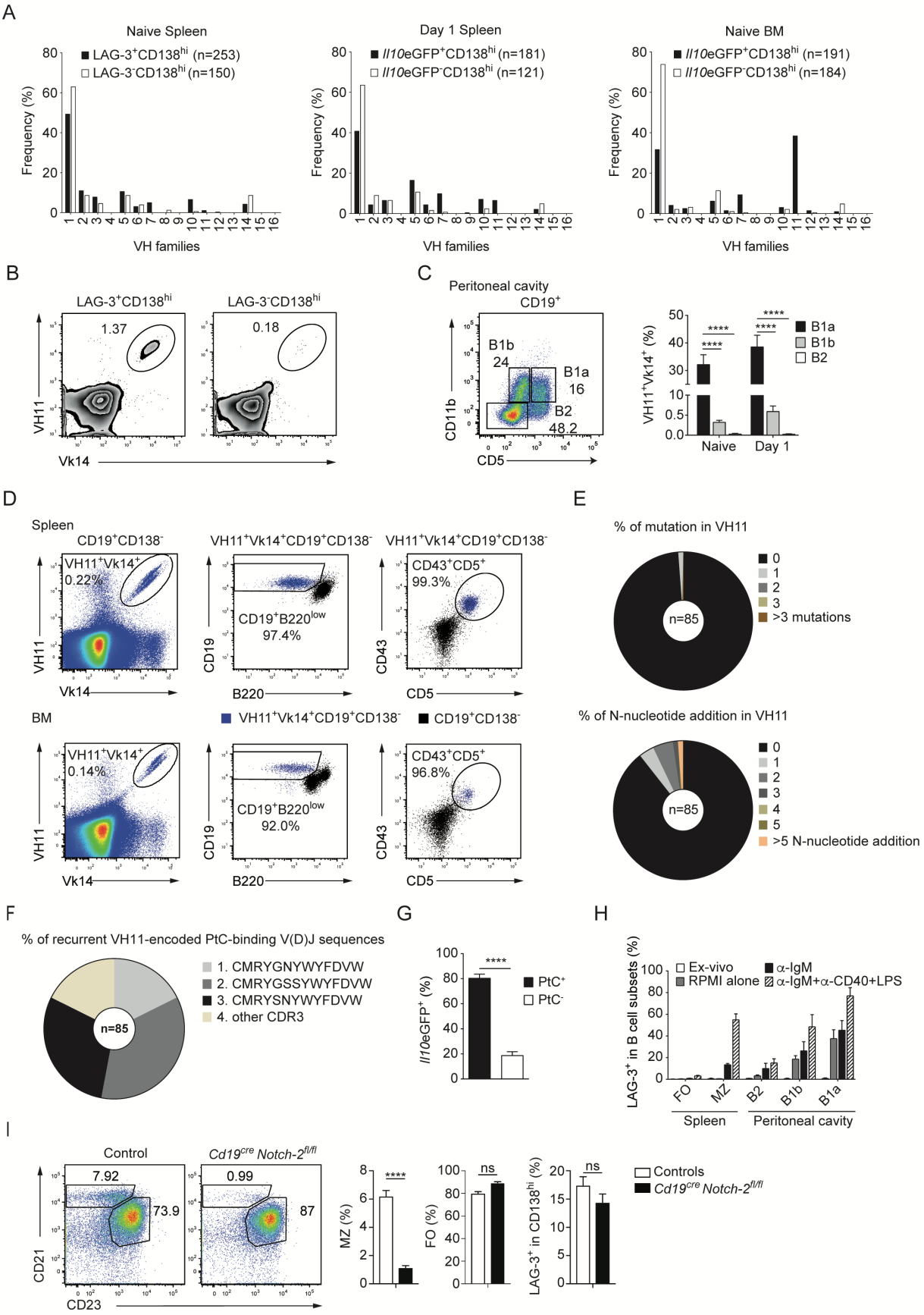
A
Naive Spleen
LAG-3+CD138hi (n=253)
LAG-3-CD138hi (n=150)
Day 1 Spleen
Il10eGFP+CD138hi (n=181)
Il10eGFP-CD138hi (n=121)
Naive BM
Il10eGFP+CD138hi (n=191)
Il10eGFP-CD138hi (n=184)
Frequency (%)
VH families
B
LAG-3+CD138hi
LAG-3-CD138hi
1.37
0.18
VH11
Vk14
C
Peritoneal cavity
CD19+
B1b
24
B1a
16
B2
48.2
CD11b
CD5
VH11+Vk14+ (%)
B1a
B1b
B2
Naive
Day 1
D
Spleen
CD19+CD138-
VH11+Vk14+CD19+CD138-
VH11+Vk14+
0.22%
CD19+B220low
97.4%
CD43+CD5+
99.3%
BM
VH11+Vk14+CD19+CD138-
CD19+CD138-
0.14%
92.0%
96.8%
E
% of mutation in VH11
n=85
0
1
2
3
>3 mutations
% of N-nucleotide addition in VH11
4
5
>5 N-nucleotide addition
F
% of recurrent VH11-encoded PtC-binding V(D)J sequences
1. CMRYGNYWYFDVW
2. CMRYGSSYWYFDVW
3. CMRYSNYWYFDVW
4. other CDR3
G
Il10eGFP+ (%)
PtC+
PtC-
H
LAG-3+ in B cell subsets (%)
Ex-vivo
RPMI alone
α-IgM
α-IgM+α-CD40+LPS
FO
MZ
B2
B1b
B1a
Spleen
Peritoneal cavity
I
Control
Cd19cre Notch-2fl/fl
7.92
73.9
0.99
87
CD21
CD23
MZ (%)
FO (%)
LAG-3+ in CD138hi (%)
ns
Controls
Cd19cre Notch-2fl/fl

Figure S5: BCR repertoire and antigen recognition properties of LAG-3- and IL-10-expressing plasmocytes, Related to Figure 5.

(A) Spleen LAG-3^{+}CD138^{hi} (naïve C57BL/6 mice, n=253) and LAG-3^{-}CD138^{hi} (naïve C57BL/6 mice, n=150), spleen *Il10*eGFP^{+}CD138^{hi} (day 1, n=181) and *Il10*eGFP^{-}CD138^{hi} (day 1, n=121), BM *Il10*eGFP^{+}CD138^{hi} (naïve, n=191) and *Il10*eGFP^{-}CD138^{hi} (naive, n=184) plasmocytes were isolated from naive and day 1-challenged mice (SL7207; 10^{7} CFU). Their *Igh* rearrangements were obtained by single cell PCR, and analysed using IMGT/V-Quest. Data show the IGHV family gene usage for the indicated populations.

(B) Representative flow cytometry plots showing the expression of VH11 and Vk14.126 on the indicated spleen cell populations from naïve (LAG-3^{+}CD138^{hi}, LAG-3^{-}CD138^{hi}) *Il10*eGFP mice.

(C) Representative flow cytometry plots showing the gating strategy to identify B1a (CD19^{+}CD11b^{+}CD5^{+}), B1b (CD19^{+}CD11b^{+}CD5^{-}) and B2 (CD19^{+}CD11b^{-}CD5^{-}) B cell subsets in PeC (gated on live CD19^{+} B cells). The histogram indicates the frequency of VH11^{+}Vk14.126^{+} among B1a, B1b and B2 subsets in naive and day 1-challenged *Il10*eGFP mice (SL7207, 10^{7} CFU). Data are pooled from 2 independent experiments (n=6 per time point).

(D) Representative flow cytometry plots showing the gating strategy to characterize VH11^{+}Vk14.126^{+} B1a cells in spleen (upper) and BM (bottom). Left plots show the expression of VH11 and Vk14.126 in CD19^{+}CD138^{-} B cells. Middle and right plots show the expression of CD19 and B220, as well as of CD43 and CD5, respectively, on VH11^{+}Vk14.126^{+}CD19^{+}CD138^{-} B cells from the spleen and BM of naïve C57BL/6 mice (in blue). The expression of these markers on CD19^{+}CD138^{-} B cells is indicated by the overlayed cells in black on the same plots. The percentages in the middle and right plots are the frequencies of CD19^{+}CD138^{-}VH11^{+}Vk14.126^{+} having the expression of CD19 and B220, as well as of CD43 and CD5, falling within the gates. Data is representative of 2 independent experiments.

(E) Frequency of IgH sequences having the indicated numbers of somatic mutations (top) or N-nucleotide additions (bottom) among all obtained VH11-positive sequences in spleen and BM from naïve and challenged mice.

(F) Frequency of IgH CDR3 sequences associated with PtC binding among all obtained VH11-positive IgH sequences in spleen and BM from naïve and challenged mice.

(G) Frequency of *Il10*eGFP^{+} cells within PtC- and non-PtC-reactive CD138^{hi} in BM from naive *Il10*eGFP mice. Data are pooled from 4 independent experiments (n=12).

(H) LAG-3 expression on B cell subsets *ex vivo*, and after overnight culture (RPMI, αIgM, αIgM+αCD40+LPS). Pools of 2-3 experiments.

(I) Flow cytometry plots and quantification of spleen B cell subsets in naïve *Cd19*-cre-*Notch2*$^{fl/f}$ mice (n=7) and littermate controls (pooled *Cd19*-cre and Notch2$^{fl/fl}$, n=8). Pool of 2 experiments (n=6).

Data show mean ± SEM. Results were compared using two-tailed unpaired t-test with Welch's correction in case of inequal variances (**** $p<0.0001$).

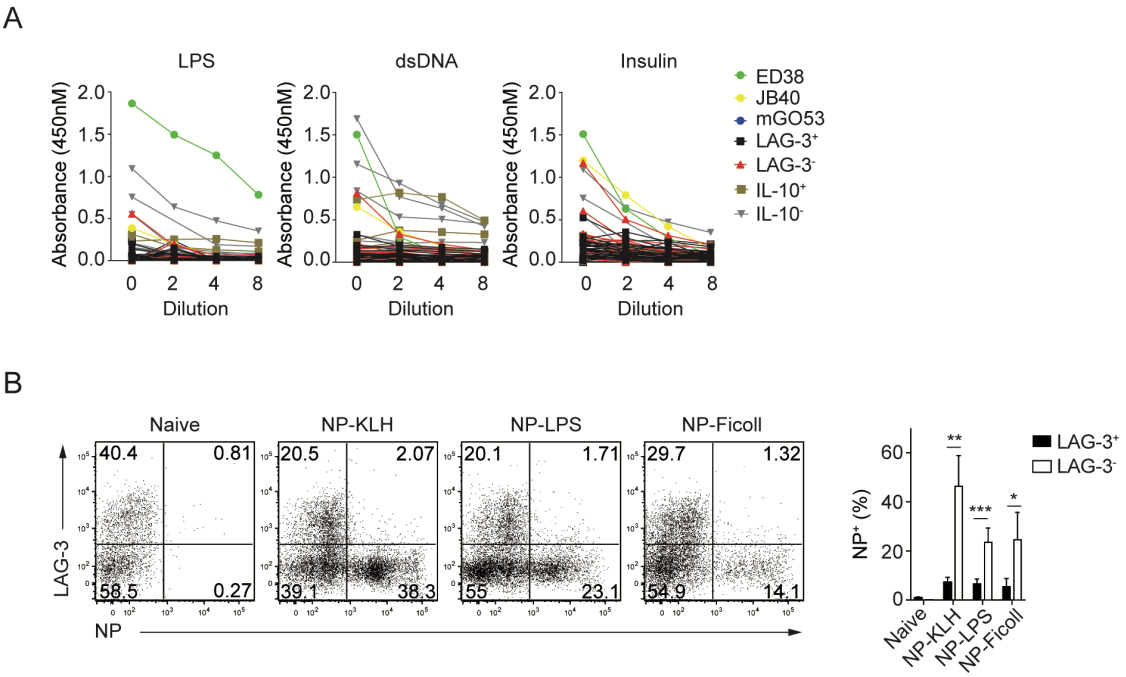

Figure S6: Reactivity of plasmocytes, Related to Figure 6.
(A) Reactivity of recombinant immunoglobulin from spleen LAG-3^{+} (n=25) and LAG-3^{-} (n=19), and BM *Il10*eGFP^{+} (n=6) as well as *Il10*eGFP^{-} (n=14) plasmocytes for LPS, dsDNA and insulin by ELISA. Green, yellow and blue lines are high positive ED38, low positive JB40, and negative control mGO53 antibodies, respectively.
(B) Flow cytometry plots showing binding of NP-allophycocyanin and expression of LAG-3 on CD138^{hi} cells from spleen of naïve and i.p. immunized mice (day 7 p.i.). Frequency of NP-binding cells within LAG-3^{+}CD138^{hi} and LAG-3^{-}CD138^{hi} spleen cells. Representative of 2 experiments (n=6). Data show mean ± SEM (*p<0.05, **p<0.01; *** p<0.001)

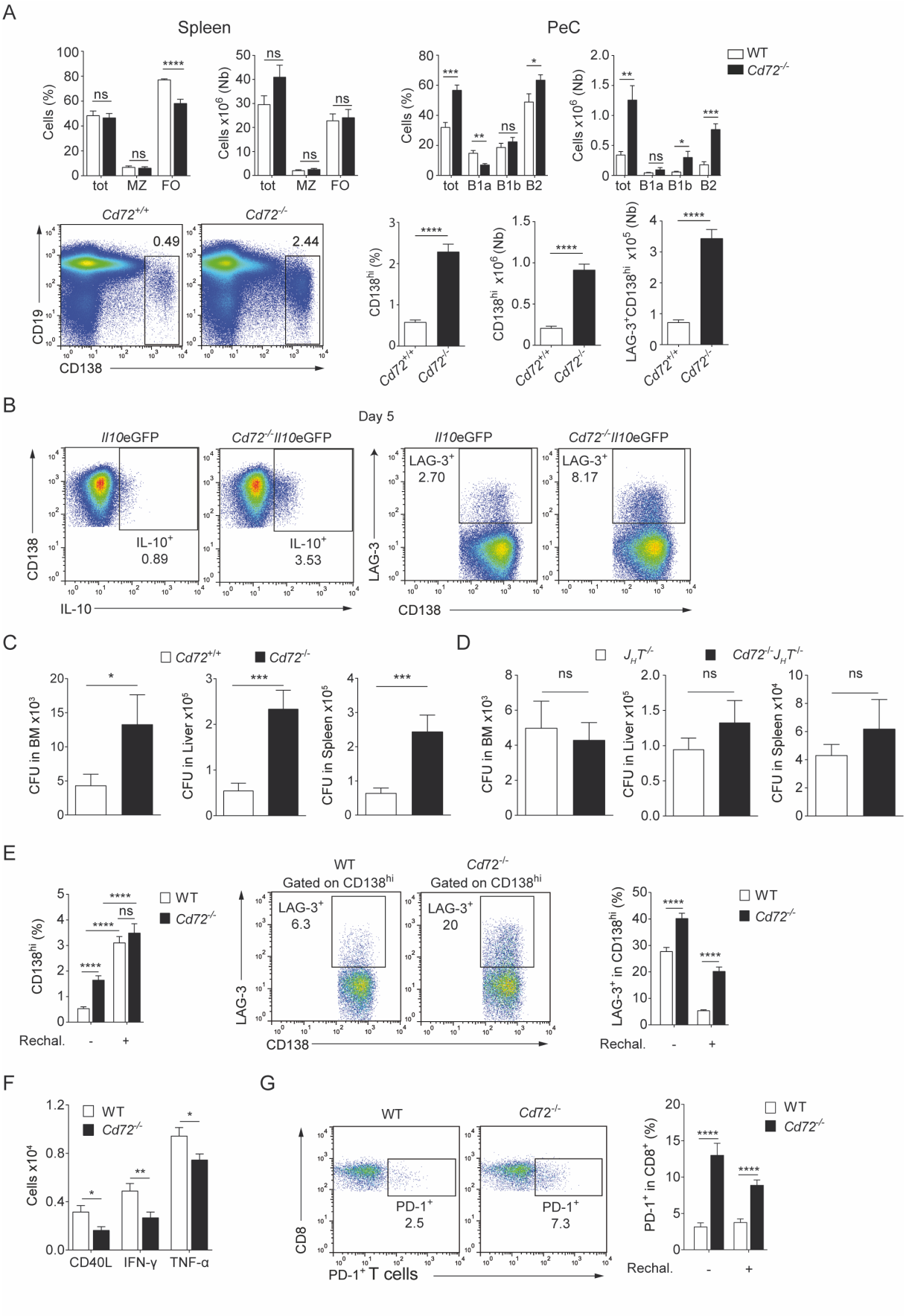
A
Spleen
PeC
WT
Cd72-/-
Cells (%)
Cells x10^6 (Nb)
tot
MZ
FO
B1a
B1b
B2
ns
Cd72+/+
Cd72-/-
0.49
2.44
CD19
CD138
CD138hi (%)
CD138hi x10^6 (Nb)
LAG-3+CD138hi x10^5 (Nb)
B
Day 5
Il10eGFP
Cd72-/-Il10eGFP
IL-10+
0.89
3.53
IL-10
LAG-3+
2.70
8.17
LAG-3
C
CFU in BM x10^3
CFU in Liver x10^5
CFU in Spleen x10^5
D
JHT-/-
Cd72-/-JHT-/-
CFU in BM x10^3
CFU in Liver x10^5
CFU in Spleen x10^4
E
CD138hi (%)
Rechal.
Gated on CD138hi
LAG-3+
6.3
20
LAG-3+ in CD138hi (%)
F
Cells x10^4
CD40L
IFN-γ
TNF-α
G
PD-1+
2.5
7.3
CD8
PD-1+ T cells
PD-1+ in CD8+ (%)

Figure S7: Host response of CD72-deficient mice during *Salmonella* infection, Related to Figure 7.
(A) Frequencies and numbers of total (tot) and indicated B cell subsets in spleen and PeC of naïve *Cd72*$^{-/-}$ and control mice. Pool of 2 experiments (n=6) (top). Flow cytometry plots and quantifications for CD138^{hi} and LAG-3^{+}CD138^{hi} cells in spleen of naïve *Cd72*$^{-/-}$ and littermate control. Pool of 3 experiments (n=13) (bottom).
(B) *Il10*eGFP and *Cd72*$^{-/-}$*Il10*eGFP shown in Figure 7A. Representative flow cytometry plots showing the expression of *Il10*eGFP and LAG-3 by CD138^{hi} cells at day 5 p.i. Data are representative from 3 independent experiments (n=9-12 per group).
(C) CFU on day 3 p.i. (SL1344, 100 CFU) for *Cd72*$^{-/-}$ and littermate controls. Pool of 5 experiments (n=22-25 per group)
(D) *Cd72*$^{-/-}$JHT (n=11) and JHT (n=10) mice were challenged with *Salmonella* (SL1344, 100 CFU). Data show CFU in BM, liver, and spleen on day 3 p.i. Data are pooled from 2 independent experiments.
(E) *Cd72*$^{-/-}$ and WT mice shown in Figure 7E. Histogram (left) shows the frequency of CD138^{hi} cells in spleen before (day 90) and 5 days after re-challenge. Representative flow cytometry plots show the expression of LAG-3 in spleen CD138^{hi} cells on day 5 after re-challenge (middle). Histogram (right) shows the frequency of LAG-3^{+} cells in CD138^{hi} cells in spleen on day 90 and day 5 after rechallenge.
(F) *Cd72*$^{-/-}$ and WT mice shown in Figure 7G. Numbers of CD40L-, IFN-γ-, and TNF-α-expressing *Salmonella*-reactive memory CD4^{+} T cells in BM on day 90 post-vaccination.
(G) *Cd72*$^{-/-}$ and WT mice shown in Figure 7H. Representative flow cytometry plots (day 95) and quantifications showing the frequency of PD-1^{+} cell in spleen CD8^{+} T cells on days 90 and 95.
Data show mean ± SEM. (^{ns}p > 0.05, *p<0.05, **p<0.01; **** p<0.0001).

Table S1. Top 50 genes that are higher expressed in naïve CD138^{hi}CD19^{+}LAG-3^{+} cells compared to naïve CD138^{hi}CD19^{+}LAG-3^{-} cells. Related to Figure 4.

Pvalue based top 50 genes that are higher expressed in naïve CD138^{hi}CD19^{+}LAG-3^{+} compared to naïve CD138^{hi}CD19^{+}LAG-3^{-}					
Rank	**Gene symbol**	**logFC**	**PValue**	**FDR**	**Synonyms**
1	Lag3	4.91	1.33E-07	0.001528	CD223|LAG-3|Ly66
2	Cpq	2.35	8.83E-07	0.002004	1190003P12Rik|2610034C17Rik|Hls2|Lal-1|Pgcp
3	Vav3	1.96	1.16E-06	0.002004	A530094I06Rik|AA986410|Idd18.1
4	Bcl2	1.67	1.4E-06	0.002004	AW986256|Bcl-2|C430015F12Rik|D630044D05Rik|D830018M01Rik
5	Zfp36l1	2.05	1.71E-06	0.002178	AW742437|AW743212|Berg36|Brf1|D530020L18Rik|ERF1|TIS11b|cMG1
6	Egr1	1.95	2.04E-06	0.002343	A530045N19Rik|ETR103|Egr-1|Krox-1|Krox-24|Krox24|NGF1-A|NGFI-A|NGFIA|TIS8|Zenk|Zfp-6|Zif268|egr
7	Inpp4a	1.89	3.49E-06	0.002981	107kDa|9630012D15|D130048C09Rik|R74740
8	Kctd12	1.45	3.66E-06	0.002981	AU046135|AW538430|Pfet1|Pfetin
9	Prg2	1.84	4.22E-06	0.002981	EMBP|MBP|mMBP|mMBP-1
10	Il4i1	2.70	4.59E-06	0.002981	Fig1|Fig1-ps|LAAO|LAO
11	Sema6d	1.91	4.65E-06	0.002981	1110067B02Rik|AA409156|D330011G23|mKIAA1479
12	Otud1	1.90	5.44E-06	0.003125	4933428L19Rik
13	Bcl2l15	1.96	6.53E-06	0.003273	Bfk|Gm566
14	Ppfibp2	1.45	6.68E-06	0.003273	Cclp1
15	Sirpa	1.32	7.47E-06	0.003273	AI835480|Bit|CD172a|P84|Ptpns1|SHP-1|SHPS-1|SIRP
16	Sell	2.59	7.49E-06	0.003273	AI528707|CD62L|L-selectin|LECAM-1|Lnhr|Ly-22|Ly-m22|Lyam-1|Lyam1
17	Jade2	1.31	8.61E-06	0.003273	1200017K05Rik|AI480685|Phf15|mKIAA0239
18	Krt222	1.45	9.23E-06	0.003273	6330509G02Rik
19	AW112010	1.97	9.69E-06	0.003273	-
20	Klf4	1.94	9.72E-06	0.003273	EZF|Gklf|Zie
21	Rgcc	1.52	1.04E-05	0.003273	1190002H23Rik|Rgc-32|Rgc32
22	Vegfa	2.01	1.06E-05	0.003273	Vegf|Vpf
23	Bhlhe40	2.58	1.08E-05	0.003273	Bhlhb2|C130042M06Rik|CR8|Clast5|Dec1|Sharp2|Stra13|Stra14
24	Ggh	2.00	1.18E-05	0.00346	gamma-GH
25	Oosp2	1.62	1.44E-05	0.003949	Gm99|Plac1l|Tmem122
26	Ly6k	1.67	1.48E-05	0.003951	2410015A16Rik|3110035B01Rik|mLy-6K
27	Cd200	1.65	1.77E-05	0.004608	Mox2|OX2
28	Serpina3f	1.45	2.06E-05	0.005062	2A1|BC049975
29	Plekha1	1.24	2.13E-05	0.005062	AA960558|C920009D07Rik|TAPP1
30	Nfkbiz	1.12	2.22E-05	0.005062	AA408868|INAP|Mail
31	Ackr3	1.92	2.25E-05	0.005062	AW541270|CXC-R7|CXCR-7|Cmkor1|Cxcr7|RDC-1|Rdc1
32	Rnf130	1.47	2.42E-05	0.005351	2510042A13Rik|G1RZFP|G1rp|GOLIATH|GP
33	Snn	1.14	2.87E-05	0.006151	2810407J07Rik|AI848521|AW547286
34	Egr2	2.55	0.00003	0.006272	Egr-2|Krox-20|Krox20|NGF1-B|Zfp-25|Zfp-6
35	Phlda1	1.47	3.24E-05	0.006652	DT1P1B11|TDAG51|Tdag
36	Il10	1.57	3.48E-05	0.006801	CSIF|Il-10
37	Ephx1	1.93	3.76E-05	0.007191	EH|Eph-1|Eph1|Epxh1|mEH
38	AB124611	1.49	5.07E-05	0.008396	Gm1706
39	Btla	1.34	0.000056	0.008941	A630002H24

40	Irf2bp2	1.15	5.77E-05	0.009071	E130305N23Rik|IRF-2BP2
41	Clec2i	1.80	5.85E-05	0.00908	Clr-g|Clrg|Dcl1|LCL-1|OCILrP2
42	Pglyrp1	1.31	6.71E-05	0.009416	PGRP|PGRP-S|Pglyrp|Tag7|Tasg7|Tnfsf3l
43	Abhd6	1.49	6.95E-05	0.009616	0610041D24Rik|AA673485|AV065425
44	Srsf7	0.89	0.000073	0.009846	35kDa|9430065L19Rik|9G8|NX-96|Sfrs7
45	Fgf1	3.38	7.36E-05	0.009846	Dffrx|Fam|Fgf-1|Fgfa
46	Ctss	1.32	0.000077	0.010022	Cats
47	Twsg1	1.26	7.88E-05	0.010022	1810013J15Rik|9030422N06Rik|AW552143|D17Ertd403e|Tsg|Twg
48	Zswim6	1.46	7.94E-05	0.010022	2900036G02Rik|mKIAA1577
49	Gpr18	1.49	8.27E-05	0.010103	-
50	Rtp4	1.62	8.39E-05	0.010104	5830458K16Rik|Ifrg28
Abbreviations					
LogFC		Log2 of fold change			
FDR		False Discovery Rate			

Table S2. Top 50 genes that are higher expressed in naïve CD138^{hi}CD19^{+}LAG-3^{-} cells compared to naïve CD138^{hi}CD19^{+}LAG-3^{+} cells. Related to Figure 4.

Pvalue based top 50 genes that are higher expressed in naïve CD138^{hi}CD19^{+}LAG-3^{-} compared to naïve CD138^{hi}CD19^{+}LAG-3^{+}					
Rank	**Gene symbol**	**logFC**	**PValue**	**FDR**	**Synonyms**
1	Ighe	-4.86	5.86E-07	0.002004	NA
2	Ighg3	-2.79	7.65E-07	0.002004	NA
3	Cdk1	-1.76	9.26E-07	0.002004	Cdc2|Cdc2a|p34<CDC2>
4	Mcm5	-1.81	1.25E-06	0.002004	AA617332|AI324988|AL033333|Cdc46|Mcmd5|P1-CDC46
5	Cdc45	-2.12	3.06E-06	0.002981	Cdc45l
6	Kpna2	-1.41	0.000004	0.002981	2410044B12Rik|IPOA1|PTAC58|Rch1
7	Ada	-1.14	4.83E-06	0.002981	-
8	Ighg2c	-3.01	4.93E-06	0.002981	NA
9	Eno1	-1.34	5.79E-06	0.003164	0610008I15|AL022784|Eno-1|MBP-1
10	Ncapg	-1.84	8.08E-06	0.003273	5730507H05Rik|Hcapg|MFT.M05.13
11	Rrm2	-1.63	8.94E-06	0.003273	AA407299|R2
12	Kif11	-1.64	9.79E-06	0.003273	Eg5|Kif8|Kifl1|Knsl1
13	Slpi	-2.10	9.81E-06	0.003273	-
14	Ighg2b	-2.66	1.03E-05	0.003273	NA
15	Ccnb2	-1.69	1.04E-05	0.003273	CycB2
16	Nuf2	-2.30	1.26E-05	0.003614	2410003C07Rik|AU044112|C85691|Cdca1|NUF2R
17	Cep55	-1.82	0.000014	0.003929	1200008O12Rik|2700032M20Rik
18	Spc24	-2.04	1.88E-05	0.004793	2410030K01Rik|AV109292|Spbc24
19	Rfc4	-1.21	0.000021	0.005062	A1|AI894123|AU040575|RFC37
20	Nmral1	-1.27	2.18E-05	0.005062	1110025F24Rik|AI256624
21	Ssr2	-1.57	2.89E-05	0.006151	1500032E05Rik|AI315033|AU020133|TLAP|TRAPB|TRAPbeta
22	Prelid1	-1.00	3.35E-05	0.006744	2610524G07Rik|Preli
23	Cdkn3	-1.82	3.49E-05	0.006801	2410006H10Rik|KAP
24	Cdc20	-1.83	4.37E-05	0.008221	2310042N09Rik|C87100|p55CDC
25	Tg	-1.33	4.74E-05	0.008396	Tgn|cog
26	Selm	-1.17	4.78E-05	0.008396	1500040L08Rik|A230103K18|Selm|Sepm
27	Ighv1-63	-2.70	4.86E-05	0.008396	NA
28	Ddost	-1.15	4.97E-05	0.008396	-
29	Ahcy	-1.19	5.06E-05	0.008396	AA987153|AL024110|CuBP|SAHH
30	Igkv4-69	-1.91	0.000051	0.008396	NA
31	NA	-3.48	5.12E-05	0.008396	NA
32	Ighv1-75	-4.83	5.12E-05	0.008396	NA
33	Top2a	-1.38	5.61E-05	0.008941	Top-2
34	Ighv15-2	-6.47	6.09E-05	0.009245	NA
35	Tigit	-1.83	6.12E-05	0.009245	ENSMUSG00000071552|Vstm3
36	H2-Eb1	-0.87	6.34E-05	0.009363	Eb|H-2Eb|H2Eb|Ia-4|Ia4
37	Spc25	-1.26	6.39E-05	0.009363	2600017H08Rik|2610205L13Rik|Spbc25
38	Kif22	-1.89	6.44E-05	0.009363	AU021460|C81217|Kid|Kif22a
39	Tcf19	-1.50	6.58E-05	0.009416	5730403J10Rik|AW495861
40	Mad2l1	-1.14	6.72E-05	0.009416	AA673185|MAD2
41	Cxcr3	-2.33	7.37E-05	0.009846	Cd183|Cmkar3
42	Igkv3-10	-1.93	7.74E-05	0.010022	NA
43	Pbk	-2.26	7.84E-05	0.010022	2810434B10Rik|AW538537|D14Ertd732e|TOPK
44	Ighv1-47	-5.14	8.04E-05	0.010035	NA
45	Dnpep	-1.03	8.16E-05	0.010078	AA407814

46	Srm	-0.92	0.000088	0.010211	AA407669|SpdST|SpdSy
47	Gstp2	-1.30	9.19E-05	0.010345	GSTpiA|Gst-3|Gst3
48	Tmem97	-1.47	9.61E-05	0.010583	1810014L12Rik|AI115531|AL022956|D11Bhm 182e
49	Shcbp1	-1.71	9.65E-05	0.010583	mPAL
50	Cenpe	-1.81	9.77E-05	0.010583	312kDa|AU019344|BC049989|C530022J18|CE NP-E|Kif10
Abbreviations					
LogFC		Log2 of fold change			
FDR		False Discovery Rate			

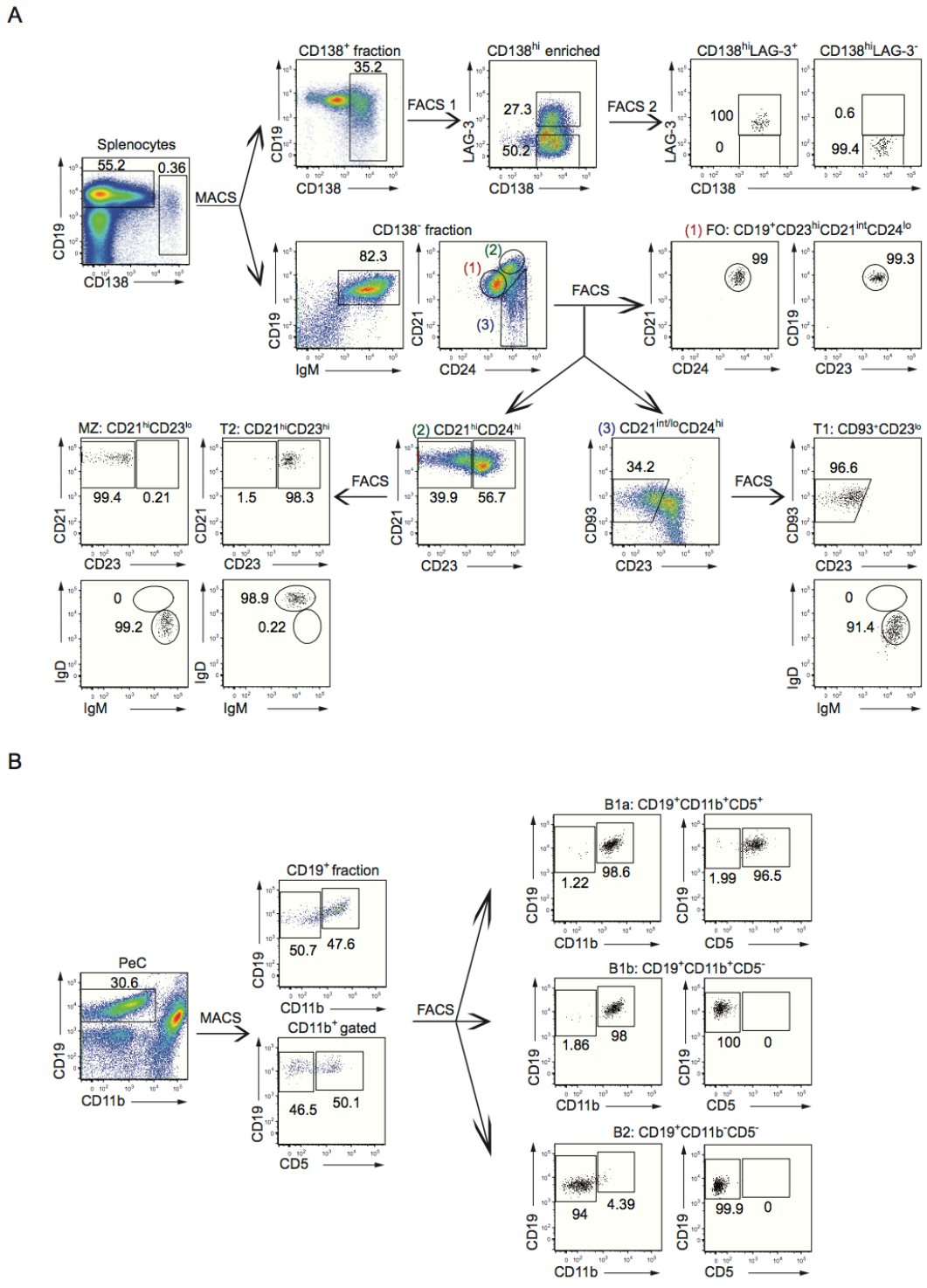

Methods S1: Strategy for the isolation of B lineage cell subsets, Related to STAR Methods
The isolation of spleen and PeC subsets are illustrated in panels A and B, respectively. For spleen, $CD138^+$ cells were first enriched by autoMACS after incubation with anti-CD138-PE (clone 281-2, BD Pharmingen) followed by anti-PE microbeads (Miltenyi Biotec). The $CD138^+$ fraction was then stained with anti-CD19, CD138, LAG-3, and CD11b/CD11c/CD3/PI. An additional enrichment of $CD138^{hi}$ cells was performed by flow cytometry sort (FACS 1), and $LAG\text{-}3^+CD138^{hi}CD11b^-CD11c^-CD3^-PI^-$ and $LAG\text{-}3^-CD138^{hi}CD11b^-CD11c^-CD3^-PI^-$ cells were then isolated by a second flow cytometry sort (FACS 2). Plasmocytes were isolated on

day 1 p.i. with 10^7 CFU *Salmonella* (SL7207) using the same strategy, according to LAG-3$^+$, LAG-3$^-$, *Il10*eGFP$^+$ and *Il10*eGFP$^-$ phenotypes. FMO controls were used to identify the LAG-3$^+$ and *Il10*eGFP$^+$ subsets. B cell subsets were isolated from the CD138$^-$ fraction obtained after autoMACS. First, T cells were depleted from the CD138$^-$ fraction by autoMACS. Follicular B cells (FO) (fraction 1 in the CD21 versus CD24 flow cytometry plot) were then isolated from this T cell-depleted CD138$^-$ fraction by flow cytometry as CD19$^+$CD23^{hi}CD21^{int}CD24^{lo}CD11b$^-$CD11c$^-$CD3$^-$PI$^-$ following staining with anti-CD19, CD21, CD23, CD24, CD11b/CD11c/CD3/PI. To obtain the other B cell subsets, the T cell-depleted CD138$^-$ fraction was stained with anti-CD19, IgM, IgD, CD21, CD23, CD24, CD93, and CD11b/CD11c/CD3/PI. Then, the fractions (2) CD19$^+$IgM$^+$CD21^{hi}CD24^{hi}CD11b$^-$CD11c$^-$CD3-PI$^-$ and (3) CD19$^+$IgM$^+$CD21$^{lo/int}$ CD24^{hi}CD11b$^-$CD11c$^-$CD3$^-$PI$^-$ were enriched by flow cytometry. The marginal zone (MZ) CD24^{hi}CD21^{hi}CD23^{lo} and transitional 2 (T2) CD24^{hi}CD21^{hi}CD23^{hi} were then sorted from fraction (2), and the transitional 1 (T1) CD24^{hi}CD21$^{lo/int}$CD23^{lo}CD93$^+$ from the fraction (3) by flow cytometry. For PeC, B cells were first purified by autoMACS via CD19-positive selection, then stained with anti-CD19, CD11b, CD5, CD11c, CD3, and PI. B1a: CD19$^+$CD11b$^+$CD5$^+$CD11c$^-$CD3$^-$PI$^-$; B1b: CD19$^+$CD11b$^+$CD5$^-$CD11c$^-$CD3$^-$PI$^-$ and B2: CD19$^+$CD11b$^-$CD5$^-$CD11c$^-$CD3$^-$PI$^-$ were then flow cytometry-sorted.